Annu. Rev. Mater. Res. 2004. 34:83–122
doi: 10.1146/annurev.matsci.34.040203.112300

First published online as a Review in Advance on February 20, 2004

SEMICONDUCTOR NANOWIRES AND NANOTUBES

Matt Law, Joshua Goldberger, and Peidong Yang
Department of Chemistry, University of California, Berkeley, California 94720; email: p_yang@uclink.berkeley.edu

Key Words heterostructure, vapor-liquid-solid process, quantum confinement

■ **Abstract** Semiconductor nanowires and nanotubes exhibit novel electronic and optical properties owing to their unique structural one-dimensionality and possible quantum confinement effects in two dimensions. With a broad selection of compositions and band structures, these one-dimensional semiconductor nanostructures are considered to be the critical components in a wide range of potential nanoscale device applications. To fully exploit these one-dimensional nanostructures, current research has focused on rational synthetic control of one-dimensional nanoscale building blocks, novel properties characterization and device fabrication based on nanowire building blocks, and integration of nanowire elements into complex functional architectures. Significant progress has been made in a few short years. This review highlights the recent advances in the field, using work from this laboratory for illustration. The understanding of general nanocrystal growth mechanisms serves as the foundation for the rational synthesis of semiconductor heterostructures in one dimension. Availability of these high-quality semiconductor nanostructures allows systematic structural-property correlation investigations, particularly of a size- and dimensionality-controlled nature. Novel properties including nanowire microcavity lasing, phonon transport, interfacial stability and chemical sensing are surveyed.

INTRODUCTION

This article is a brief account of recent progress in the synthesis, property characterization, assembly and applications of one-dimensional nanostructures, including rods, wires, belts, and tubes with lateral dimensions between 1 and 100 nm. Owing to the large amount of literature in this area, the following narrative highlights research published during 2003 and attempts to contextualize it in light of the work featured in the last review of this busy field (1). We limit our discussion to materials that have been fabricated in large quantity and with high quality using bottom-up chemical techniques; nanolithography (2) is only lightly covered. Also, carbon nanotubes and inorganic nanotubes from layered structures were recently surveyed (3, 4) and are not a focus here. This review is divided into three sections. After a brief introduction to the chemical strategies useful in synthesizing one-dimensional nanostructures, the first section explores advances in gas-phase production methods,

especially the vapor-liquid-solid (VLS) and vapor-solid (VS) processes with which most one-dimensional heterostructures and ordered arrays are now grown. We then describe several approaches for fabricating one-dimensional nanostructures in solution, focusing especially on those that utilize a selective capping mechanism. A survey of interesting fundamental properties exhibited by rods, wires, belts, and tubes is presented in the second section. In the third section, we address recent progress in the assembly of one-dimensional nanostructures into useful architectures and illustrate the construction of novel devices based on such schemes. The article concludes with an evaluation of the outstanding scientific challenges in the field and brief comments concerning the environmental and public health issues surrounding one-dimensional nanomaterials.

GENERAL SYNTHETIC STRATEGIES

An overwhelming number of articles on the synthesis of one-dimensional nanostructures was published in the past year, and it now seems inevitable that most solid-state lattices will eventually be grown in nanowire form. Rather than describe every novel nanowire stoichiometry created in 2003, we focus our discussion on the merits, limitations, and recent developments of the various synthetic strategies that are employed to form high-quality, single-crystalline nanowire materials.

Before discussing specific strategies for growing one-dimensional nanostructures, it is helpful to differentiate between growth methods and growth mechanisms. Herein, we refer to growth mechanisms as the general phenomenon whereby a one-dimensional morphology is obtained, and to growth methods as the experimentally employed chemical processes that incorporate the underlying mechanism to realize the synthesis of these nanostructures. A novel growth mechanism should satisfy three conditions: It must (*a*) explain how one-dimensional growth occurs, (*b*) provide a kinetic and thermodynamic rationale, and (*c*) be predictable and applicable to a wide variety of systems. Growth of many one-dimensional systems has been experimentally achieved without satisfactory elucidation of the underlying mechanism, as is the case for oxide nanoribbons. Nevertheless, understanding the growth mechanism is an important aspect of developing a synthetic method for generating one-dimensional nanostructures of desired material, size, and morphology. This knowledge imparts the ability to assess which of the experimental parameters controls the size, shape, and monodispersity of the nanowires, as well as the ease of tailoring the synthesis to form higher-ordered heterostructures.

In general, one-dimensional nanostructures are synthesized by promoting the crystallization of solid-state structures along one direction. The actual mechanisms of coaxing this type of crystal growth include (*a*) growth of an intrinsically anisotropic crystallographic structure, (*b*) the use of various templates with one-dimensional morphologies to direct the formation of one-dimensional nanostructures, (*c*) the introduction of a liquid/solid interface to reduce the symmetry of a seed, (*d*) use of an appropriate capping reagent to control kinetically the growth

rates of various facets of a seed, and (*e*) the self-assembly of 0D nanostructures. Many methods utilizing these growth mechanisms were not demonstrated until very recently, so many of their attributes (such as reproducibility, product uniformity and purity, potential for scaling up, cost effectiveness, and in some cases, mechanism) are poorly known. In this article, we emphasize the demonstrated performance (i.e., control of size range and flexibility in materials that can be synthesized), the intrinsic limits (i.e., limits that originate from the physics and chemistry upon which they are based), and recent advances in the growth of nanowire materials. The quality of materials is gauged by electron microscopy techniques and physical property measurements. Our emphasis is on nanowire growth resulting from the VLS, VS, and solution-phase selective capping mechanisms, as these have been shown to produce high-quality materials.

The ability to form heterostructures through carefully controlled doping and interfacing is responsible for the success of semiconductor integrated circuit technology, and the two-dimensional semiconductor interface is ubiquitous in optoelectronic devices such as light-emitting diodes (LEDs), laser diodes, quantum cascade lasers, and transistors (5). Therefore, the synthesis of one-dimensional heterostructures is equally important for potential future applications including efficient light-emitting sources and thermoelectric devices. This type of one-dimensional nanoscale heterostructure can be rationally prepared once we have a decent understanding of the fundamental one-dimensional nanostructure growth mechanism. In general, two types of one-dimensional heterostructures can be formed: longitudinal heterostructures and coaxial heterostructures. Longitudinal heterostructures refer to nanowires composed of different stoichiometries along the length of the nanowire, and coaxial heterostructures refer to nanowire materials having different core and shell compositions. Nanotubes of a variety of nonlayered lattices can be obtained by selectively etching the inner core of a coaxial heterostructure.

For convenience, we separate the synthesis section into vapor phase, solution phase, heterostructured, and nanotube processes. We first focus on the major growth mechanisms and follow with an analysis of the various synthetic methods that utilize each growth mechanism. We then discuss various approaches to fabricate heterostructure and inorganic nanotube materials derived from three-dimensional bulk crystal structures.

Growth of Nanowires from the Vapor Phase

Vapor-phase synthesis is probably the most extensively explored approach to the formation of one-dimensional nanostructures such as whiskers, nanorods, and nanowires. A vapor phase synthesis is one in which the initial starting reactants for the wire formation are gas phase species. Numerous techniques have been developed to prepare precursors into the gas phase for thin-film growth, including laser ablation, chemical vapor deposition, chemical vapor transport methods, molecular beam epitaxy, and sputtering. It should be noted that the concentrations of gaseous reactants must be carefully regulated for nanowire synthesis in order to allow

the nanowire growth mechanism to predominate and suppress secondary nucleation events. Combining these different vapor sources with an appropriate growth mechanism allows many possible permutations for synthetic design. Although the advantages and disadvantages of each vapor phase technique for thin-film growth are well known (6), their relative merits in nanowire synthesis require further investigation. For example, the specific impact of a given method on the resulting physical properties of a nanowire is not well understood, as there has yet to be a systematic experimental study detailing these effects for a specific material.

Vapor-Liquid-Solid Mechanism

Among all vapor-based methods, those employing the VLS mechanism seem to be the most successful in generating large quantities of nanowires with single-crystalline structures. This process was originally developed by Wagner & Ellis to produce micrometer-sized whiskers in the 1960s (7), later justified thermodynamically and kinetically (8), and recently reexamined by Lieber, Yang, and other researchers to generate nanowires and nanorods from a rich variety of inorganic materials (9–19). Several years ago, we used in situ transmission electron microscopy (TEM) techniques to monitor the VLS growth mechanism in real time (12). A typical VLS process starts with the dissolution of gaseous reactants into nanosized liquid droplets of a catalyst metal, followed by nucleation and growth of single-crystalline rods and then wires. The one-dimensional growth is induced and dictated by the liquid droplets, whose sizes remain essentially unchanged during the entire process of wire growth. Each liquid droplet serves as a virtual template to strictly limit the lateral growth of an individual wire. The major stages of the VLS process can be seen in Figure 1, with the growth of a Ge nanowire observed by in situ TEM. Based on the Ge-Au binary phase diagram, Ge and Au form liquid alloys when the temperature is raised above the eutectic point (361°C). Once the liquid droplet is supersaturated with Ge, nanowire growth will start to occur at the solid-liquid interface. The establishment of the symmetry-breaking solid-liquid interface is the key step for the one-dimensional nanocrystal growth in this process, whereas the stoichiometry and lattice symmetry of the semiconductor material systems are less relevant.

The growth process can be controlled in various ways. Because the diameter of each nanowire is largely determined by the size of the catalyst particle, smaller catalyst islands yield thinner nanowires. It has been demonstrated that Si and GaP nanowires of any specific size can be obtained by controlling the diameter of monodispersed gold colloids serving as the catalyst (13, 14). In general, nanowire lengths can be controlled by modifying the growth time. One of the challenges faced by the VLS process is the selection of an appropriate catalyst that will work with the solid material to be processed into one-dimensional nanostructures. Currently, this is done by analyzing the equilibrium phase diagrams. As a major requirement, there should exist a good solvent capable of forming liquid alloy with the target material, and ideally eutectic compounds should be formed. It has been shown that the analysis of catalyst and growth conditions can be

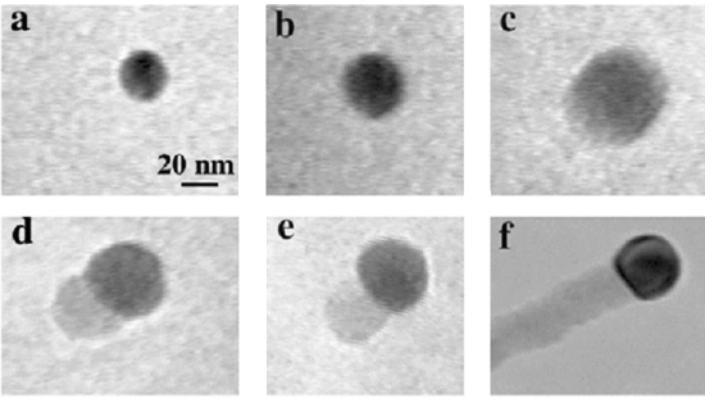

Figure 1 In situ TEM images recorded during the process of nanowire growth. (*a*) Au nanoclusters in solid state at 500°C; (*b*) alloying initiates at 800°C, at this stage Au exists mostly in solid state; (*c*) liquid Au/Ge alloy; (*d*) the nucleation of Ge nanocrystal on the alloy surface; (*e*) Ge nanocrystal elongates with further Ge condensation and eventually forms a wire (*f*). (Reprinted with permission from Reference 12, copyright Am. Chem. Soc., 2001.)

substantially simplified by considering the pseudobinary phase diagram between the metal catalyst and the solid material of interest (15). As a major limitation, it seems to be difficult to apply the VLS method to metals owing to the alloying behavior of metal and catalyst materials. The necessary use of a metal as the catalyst may also contaminate the semiconductor nanowires and thus potentially change their properties, although incorporation of metal impurities into nanowires has yet to be experimentally verified.

The VLS process has now become a widely used method for generating one-dimensional nanostructures from a rich variety of pure and doped inorganic materials that include elemental semiconductors (Si, Ge) (9–11), III–V semiconductors (GaN, GaAs, GaP, InP, InAs) (13–25), II–VI semiconductors (ZnS, ZnSe, CdS, CdSe) (26–28), oxides (indium-tin oxide, ZnO, MgO, SiO_2, CdO) (29–34), carbides (SiC, B_4C) (35, 36), and nitrides (Si_3N_4) (37). The nanowires produced using the VLS approach are remarkable for their uniformity in diameter, which is usually on the order of 10 nm over a length scale of >1 μm. Figure 2 shows scanning electron microscopy (SEM), TEM, and high-resolution transmission electron microscopy (HRTEM) images of a typical sample of GaN nanowires that was prepared using a metal organic chemical vapor deposition (MOCVD) procedure. Electron diffraction and HRTEM characterization indicate that each nanowire is essentially a single crystal. The presence of a catalyst nanoparticle at one of the ends of the nanowire (Figure 2*b*) is clear evidence supporting the VLS mechanism. However, metal droplets may not necessarily remain on the tips of VLS-made wires because interfacial dewetting and large interfacial thermal expansion differences can dislodge catalyst tips during cooling.

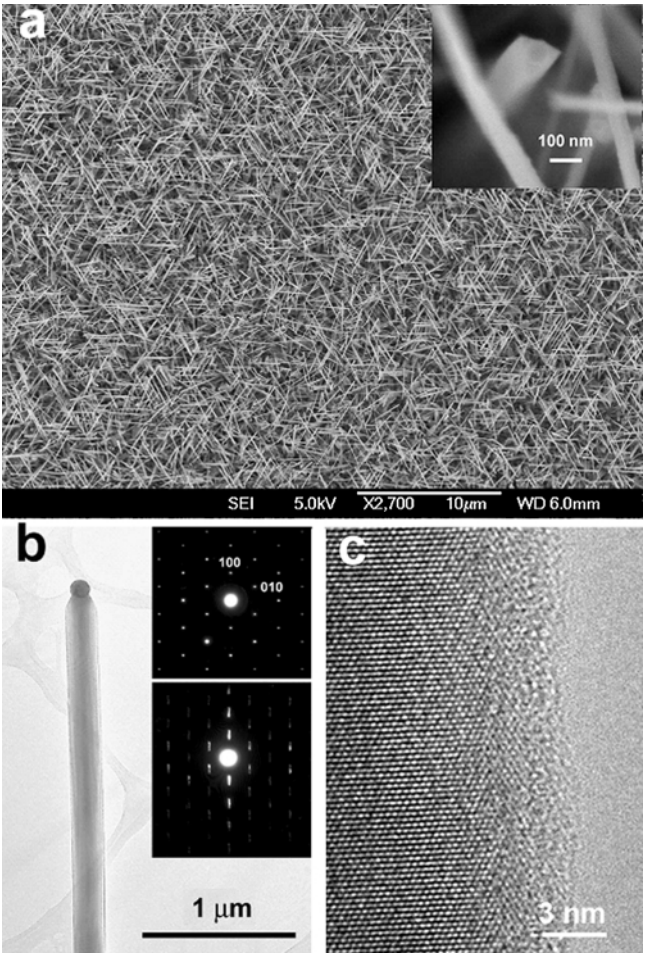

Figure 2 (*a*) Field-effect scanning electron microscope (FESEM) image of the GaN nanowires grown on a gold-coated *c*-plane sapphire substrate. Inset shows a nanowire with its triangular cross section. (*b*) TEM image of a GaN nanowire with a gold metal alloy droplet on its tip. Insets are electron diffraction patterns taken along the [001] zone axis. The lower inset is the same electron diffraction pattern but purposely defocused to reveal the wire growth direction. (*c*) Lattice-resolved TEM image of the nanowire. (Reprinted with permission from Reference 24, copyright Am. Chem. Soc., 2003.)

Self-Catalytic VLS

Because nanowires of binary and more complex stoichiometries can be created using the VLS mechanism, it is possible for one of these elements to serve as the VLS catalyst. Stach and coworkers used in situ TEM to observe directly self-catalytic growth of GaN nanowires by heating a GaN thin-film in a vacuum of

10^{-7} torr (38). It is known that GaN decomposes at temperatures above 850°C in high vacuum via the following process (39):

$$\text{GaN (s)} \rightarrow \text{Ga (l)} + 0.5\ \text{N (g)} + 0.25\ \text{N}_2\text{(g)}.$$

Also, the congruent sublimation of GaN to the diatomic or polymeric vapor species has been predicted and observed (40, 41):

$$\text{GaN (s)} \rightarrow \text{GaN (g) or } [\text{GaN}]_x\ \text{(g)}.$$

Initially, decomposition of the GaN film leads to the formation of isolated liquid Ga nanoparticles. The resultant vapor species, composed of the atomic nitrogen and diatomic or polymeric GaN, then redissolves into the Ga droplets and initiates VLS nanowire after supersaturating the metal and establishing a liquid-Ga/solid-GaN interface. Each step in the VLS process was observed in this TEM study (Figure 3): the alloying of the Ga droplet with the nitrogen-rich vapor species, the nucleation of the nanowire liquid-metal interface, and the subsequent axial nanowire growth.

The major advantage of a self-catalytic process is that it avoids undesired contamination from foreign metal atoms typically used as VLS catalysts. Self-catalytic behavior has been reported when the direct reaction of Ga with NH_3 or direct evaporation of GaN was used to produce GaN nanowires (18, 42). The precise control of nanowire lengths and diameters using a self-catalytic VLS technique, as well as the universality of this approach, has yet to be demonstrated.

VLS Vapor Phase Methods

For a specific material, the dependence that the method of introducing vapor species has on the nanowire physical properties has not been systematically studied. Certain methods of introducing vapor phase precursors will allow a much greater flexibility in dopant selection, as well give greater control over the compound stoichiometry. Furthermore, integration of nanowire components into current thin-film technologies is an important consideration. Specific vapor phase methods (such as MOCVD) will be more compatible with process integration than others.

To demonstrate these points, let us consider the case of GaN nanowires. Synthetic schemes for GaN-based devices have employed laser ablation (43, 44), chemical vapor transport (16, 25, 45–48), and most recently, MOCVD (24). The highest carrier mobility values are reported for thin films grown by MOCVD, hydride phase vapor epitaxy, or molecular beam expitaxy (MBE). Of these methods, MOCVD should allow the greatest flexibility for producing nanowires with controlled dopant and other ternary nitride phase concentrations. This is partly because of the similarity of the precursor chemistries for the constituent and dopant atoms. Finally, MOCVD is on the same technical platform as thin-film technologies and thus can be easily integrated into existing GaN thin-film technologies.

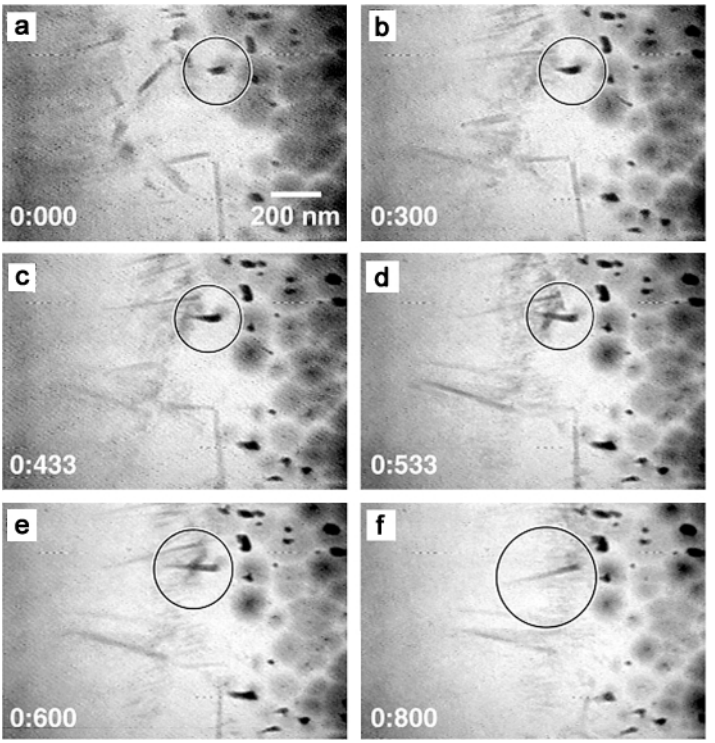

Figure 3 A series of video frames grabbed from observations of GaN decomposition at ~1050°C, showing the real-time GaN nanowire growth process. The number on the bottom left corner of each frame is the time (second:millisecond). (Reprinted with permission from Reference 38, copyright Am. Chem. Soc., 2003).

Vapor-Solid Growth Mechanisms

There have been numerous reports on one-dimensional nanostructure formation from vapor phase precursors in the absence of a metal catalyst or obvious VLS evidence (49). Herein we refer to this synthetic method of creating one-dimensional materials as the vapor-solid method. There are many plausible growth mechanisms to consider, and a synthetic experiment might produce nanostructures grown from a combination of these mechanisms. Using thermodynamic and kinetic considerations, the formation of nanowires could be possibly through (*a*) an anisotropic growth mechanism, (*b*) Frank's screw dislocation mechanism (50), (*c*) a different defect-induced growth model, or (*d*) self-catalytic VLS. In an anisotropic growth mechanism, one-dimensional growth can be accomplished by the preferential reactivity and binding of gas phase reactants along specific crystal facets (thermodynamic and kinetic parameters) and also the desire for a system to minimize surface energies (thermodynamic parameter). In the dislocation and defect-induced growth models, specific defects (for example screw dislocations) are known to

have larger sticking coefficients for gas phase species, thus allowing enhanced reactivity and deposition of gas phase reactants at these defects. Other recently proposed vapor-solid growth mechanisms have been reported, for example the oxide-assisted growth mechanism (51). However, many of these proposed vapor-solid growth mechanisms lack compelling thermodynamic and kinetic justification of one-dimensional growth; careful experiments are needed in order to unravel the fundamental nanowire growth events under these conditions.

Although the exact mechanisms responsible for vapor-solid growth are not completely elucidated, many materials with interesting morphologies have been made using these methods. Most significantly, the Wang group has created nanoribbon materials (of ZnO, SnO_2, In_2O_3, and CdO) having rectangular cross sections by simply evaporating commercial metal oxide powders at elevated temperatures (52). These nanoribbons are structurally uniform, with typical thicknesses from 30 to 300 nm, width-to-thickness ratios of 5–10, and lengths up to several millimeters (49). Finally, vapor-solid methods have been utilized to form a variety of more complex morphologies. For instance, we have used this method to create ZnO tetrapods and comb-like morphologies (53, 54).

Nanowire Growth in Solution

A few of the major disadvantages of high-temperature approaches to nanowire synthesis include the high cost of fabrication and scale-up and the inability to produce metallic wires. Recent progress using solution-phase techniques has resulted in the creation of one-dimensional nanostructures in high yields (gram scales) via selective capping mechanisms. It is believed that molecular capping agents play a significant role in the kinetic control of the nanocrystal growth by preferentially adsorbing to specific crystal faces, thus inhibiting growth of that surface (although defects could also induce such one-dimensional crystal growth).

Evidence for this selective capping mechanism has been recently documented by Sun et al. (55) in the formation of silver nanowires using poly(vinyl pyrrolidone) (PVP) as a capping agent. In the presence of PVP, most silver particles can be directed to grow into nanowires with uniform diameters. One possible explanation is that PVP selectively binds to the $\{100\}$ facets of silver while maintaining $\{111\}$ facets to allow growth. To demonstrate this selective passivation of Ag nanowires along the $\{100\}$ faces, Sun et al. functionalized their nanowires post-growth under mild conditions with a dithiol compound, and subsequently added gold nanoparticles to the solution. They found that the gold nanoparticles bonded only to the end $\{111\}$ caps, thereby showing only dithiol adhesion on the ends caps and not the $\{100\}$ faces owing to the preferential bonding of the PVP to these faces.

In this process Sun et al. generated nanowires of silver with diameters in the range of 30–60 nm and lengths up to $\sim$50 μm. This work on silver, together with previous studies on gold and other metals, suggests that many metals can be processed as nanowires through solution-phase methods by finding a chemical reagent capable of selectively interacting with various surfaces of a metal.

The growth of semiconductor nanowires has also been realized using a similar synthetic mechanism. Microrods of ZnO have been produced via the hydrolysis

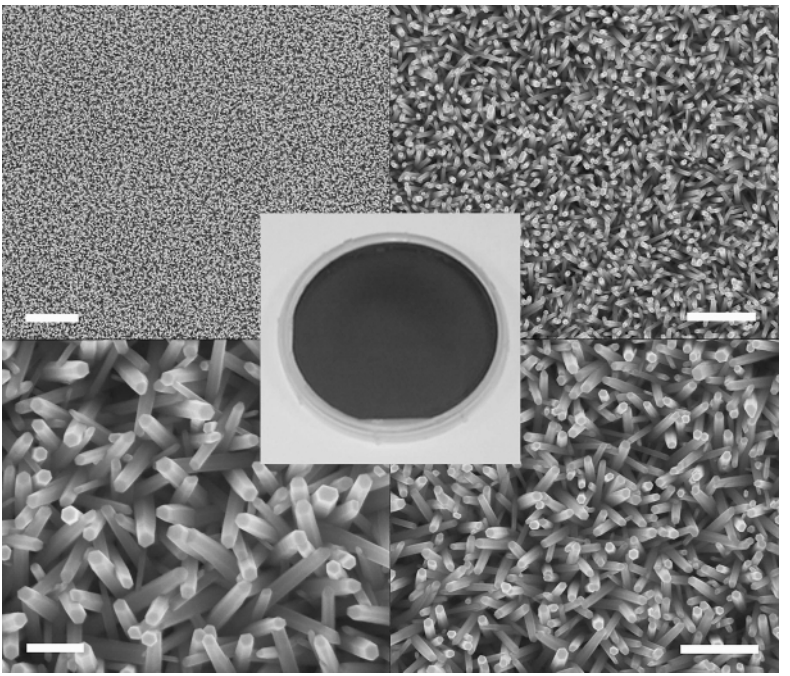

Figure 4 ZnO nanowire array on a 4-inch silicon wafer. Centered is a photograph of a coated wafer, surrounded by SEM images of the array at different locations and magnifications. These images are representative of the entire surface. Scale bars, clockwise from upper left, correspond to 2 μm, 1 μm, 500 nm, and 200 nm. (Reprinted with permission from Reference 57, copyright Wiley-VCH, 2003.)

of zinc salts in the presence of amines (56). Following this work, we used hexamethylenetetramine as a structural director to produce dense arrays of ZnO nanowires in aqueous solution (Figure 4) having controllable diameters of 30–100 nm and lengths of 2–10 μm (57). Most significantly, these oriented nanowires can be prepared on any substrate. The growth process ensures that a majority of the nanowires in the array are in direct contact with the substrate and provide a continuous pathway for carrier transport, an important feature for future electronic devices based on these materials.

A major limitation of this growth mechanism is that most capping agents are chosen via an empirical trial-and-error approach. It would therefore be advantageous to develop a library of bond strengths of various chemisorbed capping agents on specific crystal planes.

Longitudinal Heterostructures

The growth of longitudinal heterostructured nanowires involves using a single one-dimensional growth mechanism that can be easily switched between different

materials mid-growth. In order to obtain technologically useful heterostructures, the growth mechanism must be compatible with the desired materials and produce well-defined and coherent interfaces with good control. Because the VLS growth mechanism can readily provide such control, most work involving longitudinal heterostructure synthesis has been performed using this approach.

Researchers in our laboratory recently demonstrated the use of a hybrid pulsed laser ablation/chemical vapor deposition (PLA-CVD) process for generating semiconductor nanowires with periodic longitudinal heterostructures (58). In this process, Si and Ge vapor sources are independently controlled and alternately delivered into the VLS nanowire growth system. As a result, single-crystalline nanowires containing the Si/SiGe superlattice structure are obtained.

Figure 5 shows a TEM image of two such nanowires in the bright-field mode. Dark stripes appear periodically along the longitudinal axis of each wire, reflecting the alternating domains of Si and SiGe alloy. Because the electron scattering cross section of Ge is larger than that of Si, the SiGe alloy block appears darker than the pure Si block. The chemical composition of the dark region was also examined

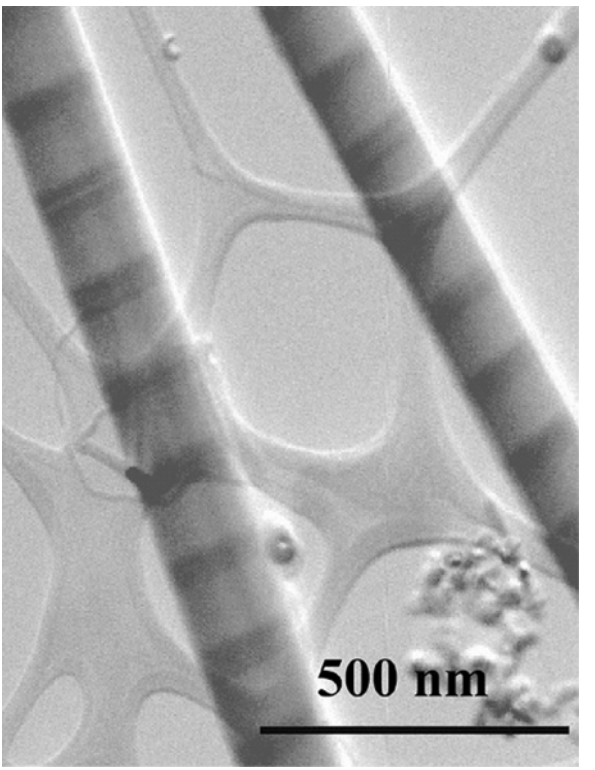

Figure 5 Transmission electron microscopy (TEM) image of two Si/SiGe superlattice nanowires.

using energy-dispersive X-ray spectroscopy (EDS), showing a strong Si peak and apparent Ge doping (~12 wt% Ge). The Si and Ge signals are periodically modulated with anticorrelated intensities. This observation also supports the formation of a Si/SiGe superlattice along the wire axis.

Using a similar approach, the Lieber and Samuelson groups prepared GaAs/GaP and InAs/InP heterostructured nanowires, respectively (59, 60). Furthermore, Solanki and colleagues have recently reported the ability to produce ZnSe/CdSe superlattice nanowires (61). Because the supply of vapor sources can be readily programmed, the VLS process with modulated sources is useful for preparing a variety of heterostructures on individual nanowires in a custom-designed fashion. It also enables the creation of various functional devices (e.g., *p-n* junctions, coupled quantum dot structures, and heterostructured unipolar and bipolar transistors) on individual nanowires. These heterostructured nanowires can be further used as important building blocks to construct nanoscale electronic circuits and light-emitting devices.

There have been a few recent reports on the synthesis of longitudinal nanowire heterostructures synthesized using a non-VLS mechanism. Keating & Natan and Valizadeh et al. have, respectively, fabricated striped Ag/Au and Au/Co nanowire superlattices using a sequential electrochemical method inside anodic aluminum oxide templates (62, 63). Finally, Kim et al. recently synthesized GaN *p-n* junctions using a chemical vapor transport vapor-solid process by introducing the p-type dopant Cp_2Mg mid-growth (48).

Coaxial Heterostructures

Coaxial nanowires, a second class of nanowire heterostructures, are both fundamentally interesting and have significant technological potential. Coaxial structures can be fabricated by coating an array of nanowires with a conformal layer of a second material. The coating method chosen should allow excellent uniformity and control of the sheath thickness. Cladding nanowires with amorphous layers of SiO_2 or carbon is synthetically facile and routinely demonstrated in the literature. A more exciting and difficult task, with greater technological import, is to form heterostructures of two single-crystalline semiconductor materials. We reported the synthesis of GaN/$Al_{0.75}Ga_{0.25}N$ core-sheath structures using a chemical vapor transport method (Figure 6) (46). Shortly thereafter, ZnO/GaN core-sheath heterostructures were grown by our laboratory using a MOCVD approach (64). Also, the Lieber group has studied Si/Ge core-sheath wires produced by chemical vapor deposition methods (65). It is important to point out that the choice of appropriate core and sheath materials with similar crystallographic symmetries and lattice constants is essential to achieve the deposition of single-crystalline epitaxial thin-film sheath structures and thereby produce high-quality materials.

Similar to the concept of creating a uniform sheath around a nanowire is the idea of coating one-dimensional nanostructures anisotropically, i.e., only along one side of the nanowire material. We have developed a versatile approach to the synthesis

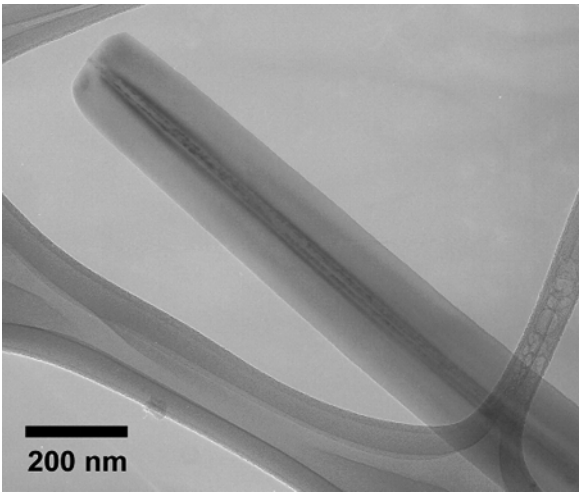

Figure 6 Transmission electron microscopy image of a GaN/AlGaN core-sheath nanowire.

of composite nanowire structures where the composition limitation is relaxed and the resulting nanostructures could readily have multiple functionalities such as luminescence, ferromagnetism, ferroelectric, or superconducting properties (66). In this process, tin dioxide nanoribbons were used as substrates for the thin-film growth of various oxides (e.g., TiO_2, transition metal doped TiO_2, and ZnO) using pulsed laser deposition (PLD). The energetic nature of the laser ablation process makes the plume highly directional and enables selective film deposition on one side of the nanoribbon substrate via the shadow effect (Figure 7). Electron microscopy and X-ray diffraction studies demonstrate that these functional oxides can grow epitaxially on the side surfaces of the substrate nanoribbons with sharp structural and compositional interfaces.

Nanotube Formation

There have been numerous studies on the synthesis of inorganic nanotubes derived from materials with layered bulk crystal structures, including C, BN, MoS_2, WS_2, V_2O_5, $H_3Ti_2O_7$, etc. (4). The creation of epitaxial core-sheath structures imparts the ability to synthesize single-crystalline nanotube materials derived from three-dimensional crystal structures by dissolving the inner core. This synthetic approach requires that the core and sheath materials exist in epitaxial registry and possess differing chemical stability.

This "epitaxial casting" strategy was used to synthesize GaN nanotubes with inner diameters of 30–200 nm and wall thicknesses of 5–50 nm (64). Hexagonal ZnO nanowires were used as templates for the epitaxial overgrowth of thin GaN

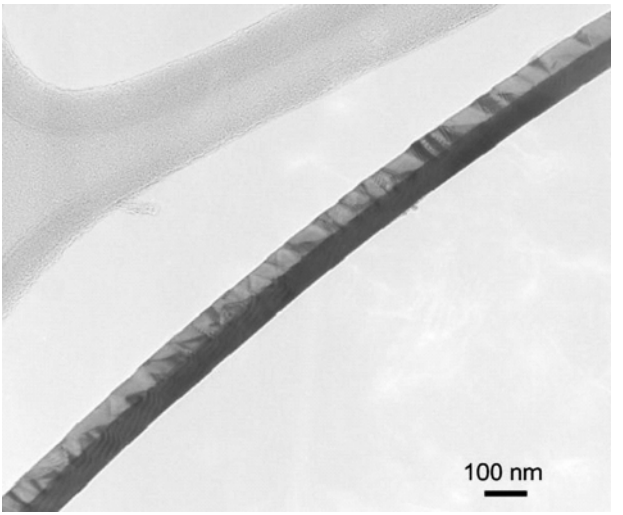

Figure 7 Transmission electron microscopy image of a highly crystalline SnO_2/TiO_2 composite nanoribbon showing the epitaxial growth of TiO_2 on the SnO_2 nanoribbon surface.

layers in a MOCVD system. The ZnO nanowire templates were subsequently removed by simple thermal reduction and evaporation in NH_3/H_2 mixtures, which resulted in ordered arrays of GaN nanotubes on the substrate. This is the first example of single-crystalline GaN nanotubes and this novel templating process should be applicable to many other semiconductor systems (Figure 8).

Related to this approach, amorphous SiO_2 nanotubes with controlled shell thicknesses were recently synthesized from silicon nanowire templates. In this work, Si nanowires were thermally oxidized at different temperatures to give uniform oxide sheath thicknesses, and the inner Si nanowires were then etched away with XeF_2 to yield silica tubes (67). Subsequent reports of the synthesis of nonlayered nanotubular materials include AlN (68) and In_2O_3 (69). The mechanisms of nanotube formation via these latter methods are not well established. These direct approaches do not give the same level of control over nanotube positioning and shell thickness uniformity as is possible with epitaxial casting.

NOVEL PROPERTIES OF SEMICONDUCTOR NANOWIRES

Quantum Confinement

By now the phenomenon of charge carrier confinement in quantum dots, wires, and wells is familiar to researchers working with nanostructures. Quantum confinement is approximately described by simple particle-in-a-box type models, and its most distinctive signature is the $1/d^n$ (where d is the diameter and $1 \leq n \leq 2$) size

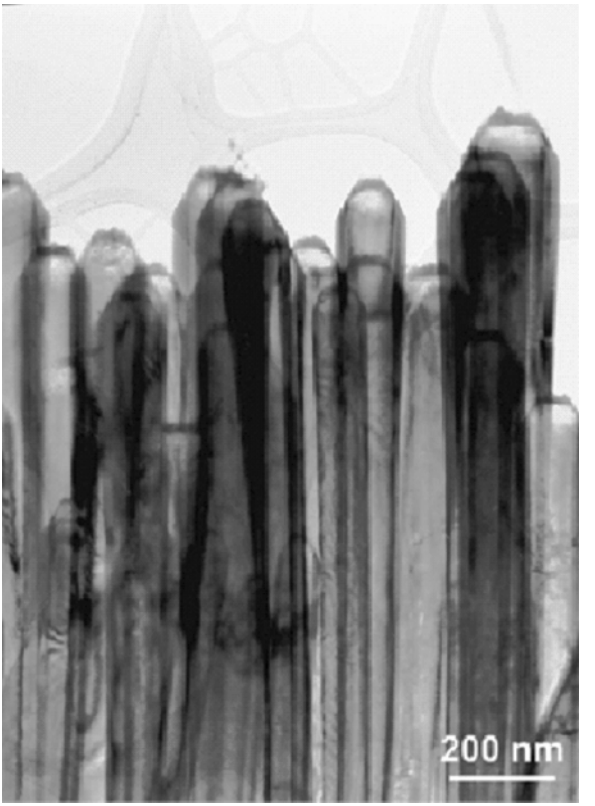

Figure 8 Transmission electron microscopy image of a cluster of single-crystalline GaN nanotubes prepared using the epitaxial casting methodology.

dependence of the bandgap in semiconductors. A recent detailed study of the effect of dimensionality on confinement in InP dots and wires (70) concluded that the size dependence of the bandgap in wires is weaker than in dots by the amount expected from simple theory. However, the absolute bandgap shifts in InP dots ($\Delta E_g \sim 1/d^{1.35}$) and wires ($\Delta E_g \sim 1/d^{1.45}$) did not follow the particle-in-a-box prediction (i.e., $1/d^2$), demonstrating that accurate treatments of confinement require higher-order calculations to account for band structure. Most experimental investigations of quantum confinement focus on its optical effects.

Bandgap tunability and the resulting shifts in absorption/emission energies have been extensively researched in nanoparticles (71) and in homogeneous nanorods made of materials with reasonably large exciton Bohr radii, such as CdSe (72) and InAs (73). Single InP nanowires have also received attention (74). The photoluminescence (PL) of well-dispersed, size-selected InP wires was found to blueshift with decreasing size for diameters less than 20 nm. Light absorption and emission

in a nanowire is highly polarization dependent such that the PL intensity is a maximum for polarization parallel to the long axis of the nanowire (75, 76). This polarization anisotropy is likely due to the sharp dielectric contrast between a nanowire and its surroundings, which can be exploited to create polarization-sensitive photodetectors and other devices.

Quantum-confined one-dimensional nanostructures are strong candidates for use in photovoltaic devices based on blended composites. In a proof of concept study (77), Alivisatos and coworkers mixed CdSe nanorods with polythiophenes to create solar cells with power conversion efficiencies as high as 1.7%. The nanorods in these cells function as light absorbers, charge separation interfaces, and electron-transporting elements. Improving the transport network by replacing nanorods with CdTe tetrapod-branched nanocrystals (78) should enhance future cell performance. Furthermore, the overlap of the CdTe absorption profile with the solar spectrum is tunable by ~0.5 eV by altering the diameter of the four arms of the tetrapods, thereby enabling the band engineering of a single-junction solar cell.

The ability to fabricate nanoscale heterostructures in the form of periodic quantum wells imbedded in a nanowire or rod could enable many new device applications, particularly in optoelectronics. The ZnO/ZnMgO multiple quantum well (MQW) nanorod study by Pennycook and colleagues (79) is a fine example of a versatile quantum device based on an individual heterostructure. They used metal-organic vapor phase epitaxy (MOVPE) to grow nanorods containing a sequence of thin ZnO wells separated by epitaxial $Zn_{0.8}Mg_{0.2}O$ layers. Continuous tuning of the emission wavelength from 3.36 eV to 3.515 eV was possible by thinning the well width from 11 to 1.1 nm. ZnO is one of the few oxides that show quantum confinement effects in an experimentally accessible size range (<8 nm).

In addition to true MQW one-dimensional objects, confined core-sheath nanowire heterostructures provide a unique geometry for applications in optoelectronics. We recently demonstrated UV lasing from optically pumped GaN/$Al_xGa_{1-x}N$ core-sheath quantum wires (46). Phase separation during the VLS process leads to cylindrical GaN cores with diameters as small as 5 nm cladded by a 50–100-nm layer of $Al_{0.75}Ga_{0.25}N$. Normally, GaN nanowires with diameters less than ~100 nm are too leaky to sustain laser cavity modes. Surrounding slender GaN wires with a material of larger bandgap and smaller refractive index creates a structure with simultaneous exciton and photon confinement (waveguiding). When optically pumped, the core provides a gain medium and the sheath acts as a Fabry-Perot optical cavity. We found that PL and lasing emission was blueshifted from the bulk (Figure 9), with lasing thresholds roughly ten times higher than those of larger, unclad GaN nanowire lasers.

In addition to the exciton Bohr radius, there are several other characteristic lengths for physical phenomena that typically fall in the range of 1–500 nm (Figure 10), such as the phonon and electron mean free paths, the Debye length, and the exciton diffusion length for certain polymers. It is clear that chemically synthesized nanowires 5–100 nm in diameter should allow experimental access to a rich spectrum of these mesoscopic phenomena.

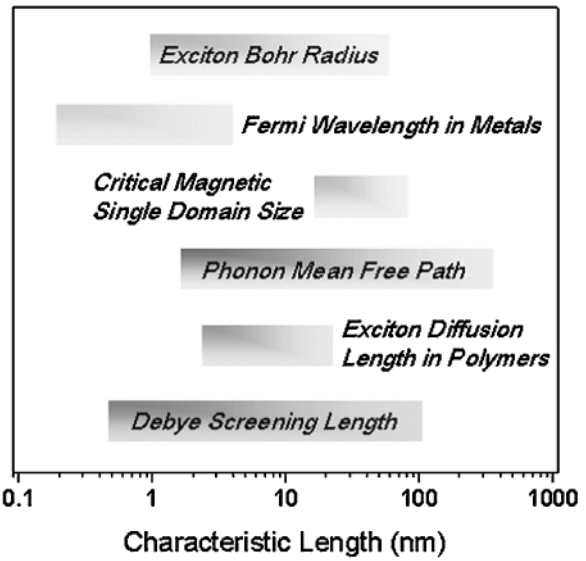

Figure 10 A few characteristic length scales for condensed systems at 300 K. Chemically synthesized nanowires 5–100 nm in diameter allow experimental access to a rich spectrum of mesoscopic phenomena.

Mechanical and Thermal Stability

The small sizes and high surface-to-volume ratios of one-dimensional nanostructures endow them with a variety of interesting and useful mechanical properties. Their high stiffness and strength lend them to applications in tough composites and as nanoscale actuators, force sensors and calorimeters. One-dimensional nanostructures also showcase unique stability effects driven by the dominance of their surfaces and internal interfaces.

One of the most familiar mechanical phenomenon involving size dependency is the Hall-Petch effect characteristic of polycrystalline solids. The yield strength and hardness of a microstructured polycrystalline material typically increase with decreasing grain size owing to the progressively more effective disruption of dislocation motion by grain boundaries. However, recent studies on solids composed of nanoscale grains suggest that the Hall-Petch relation breaks down at a critical grain size, below which a material softens. Atomistic modeling carried out by Schiotz (80) points to a transition from dislocation-mediated yielding to grain boundary sliding at very small crystallite sizes as the primary explanation for the anomalous maximum in the strength of metallic polycrystalline solids. The mechanics involved in the simulations are subtle and need to be confirmed and explored in careful experiments on films and freestanding one-dimensional structures.

As the scale of materials reduces to nanometers, the tendency of surfaces to minimize their free energy may drive structural changes that propagate into the bulk. Surface-induced global reconstruction has been observed and modeled in freestanding nanofilms of various metals, particularly gold (81). These studies show that at a critical thickness, face-centered-cubic (f.c.c.) metal films with $\{100\}$ orientations restructure to a low-energy $\{111\}$ orientation to relieve the large tensile stress present in the $\{100\}$ surfaces of these materials. Recently, Diao and colleagues have explored this phenomenon in gold nanowires using atomistic simulations (82). They report a spontaneous f.c.c. to body-centered-tetragonal phase transition in nanowires with a $\langle 100 \rangle$ initial crystal orientation and cross-sectional area below 4 nm^2. The transition is nucleated at the ends of the nanowire and propagates inward at a tenth the speed of sound in gold. No such effect was found in wires with $\langle 110 \rangle$ or $\langle 111 \rangle$ growth directions, as these orientations feature surfaces that lack sufficient stress to overcome bulk stability. The detailed nature and extent of this dramatic effect in one-dimensional nanostructures is largely an open area for experimentation.

It is known that the melting temperature of a crystal is inversely proportional to its effective radius for grains smaller than 20 to 40 nm (83–85). This effect is a consequence of the large fraction of atoms with low coordination numbers present in solids with high surface-to-volume ratios. So far, there is no experimental verification of size-dependent thermal melting in thin one-dimensional nanostructures, principally owing to the difficulty of fabricating freestanding rods or wires with <10 nm diameter. Photo-induced melting and fragmentation of metal nanorods in solution has been studied in detail using femto- to nanosecond light pulses (86, 87). Also, a large melting point depression was reported in the case of germanium nanowires (10–100 nm in diameter) encased in carbon sheaths (88). TEM showed that the ends of sheathed wires began to melt 280°C below the bulk melting temperature, with the liquid fronts meeting in the middle $\sim$80°C shy of the bulk value. The latter study is a nanowire example of capillary melting (89) (the Gibbs-Thomson effect), in which the solid-liquid equilibrium of a material is shifted to lower temperature by confinement in a sheath having good wetting properties with the liquid.

Interface-driven instability is a key feature of both freestanding and encapsulated one-dimensional nanostructures, but perhaps its most technologically relevant appearance is in nanowire films confined to nanowire substrates. Work in this laboratory (M. Law, X. Zhang, R. Yu & P. Yang, unpublished results) has focused on the thermal properties of bilayer nanoribbons as analogues for important nanoscale interfaces such as the silicon-aluminum contact in nanoelectronics. By perturbing and monitoring individual bilayers using in situ TEM, it is possible to study the details of interfacial processes such as diffusion, electromigration, grain growth, melting, and reaction between two well-defined as-deposited materials. For example, the slow heating of Cu-SnO_2 bilayer nanoribbons causes interfacial stress that bends the structures elastically at temperatures <200°C. At intermediate temperatures, the initially smooth Cu layer thickens and breaks up into three-dimensional

islands as this thermodynamically preferred wetting state becomes thermally accessible. Finally, reduction of the SnO_2 substrate by Cu at $\sim$550°C leads to etching of the interface and the appearance of several new phases.

Nanowire synthesis techniques can yield single-crystalline structures with a much lower density of line defects than is typically found in bulk materials. As a result, one-dimensional nanostructures often feature a mechanical strength, stiffness, and toughness approaching the theoretical limits of perfect crystals, making them attractive for use in composites and as actuators in nanoelectromechanical systems (NEMS). In 1997, the Lieber group pioneered the use of atomic force microscopy (AFM) to determine the mechanical properties of individual SiC nanorods that were pinned at one end to a solid substrate (91). AFM studies on SiC rods and MoS_2 tubes (92) measuring force-displacement relations yielded Young's moduli near their theoretical maxima. Wang and coworkers demonstrated an alternative method for determining the elastic properties of one-dimensional nanostructures based on electric-field-induced resonant excitation of single SiC/SiO_2 (93) wires and ZnO (94) belts in situ in a TEM. By applying an alternating electric field tuned to the natural vibration frequency of a ZnO belt pinned at one end to a TEM grid, the researchers found that the quasi-rectangular belts exhibited dual fundamental frequencies and an average bending modulus of 52 GPa, close to the theoretical value.

In addition to mechanical characterization, several studies have demonstrated mechanical actuation based on the unique features of one-dimensional structures. For instance, flexible SiO_2 helices heated by an electron beam show expansion-contraction behavior similar to that of a spring (95). In recent work, entangled sheets of V_2O_5 nanowires have been used as electromechanical actuators in liquid media (96). The large surface area and Young's modulus of the freestanding sheets are key to their ability to generate substantial forces (5.9 MPa) in response to reversible cation intercalation and double-layer charging. A separate study has explored the thermomechanical bending of bilayer ribbons via the well-known bimetallic effect (M. Law, T. Kuykendall, X. Zhang & P. Yang, unpublished results). It was shown that epitaxial Cu-SnO_2 bilayers act as reversible thermal switches at temperatures $<$200°C, with tip displacements of several hundred nanometers as monitored by TEM. The use of more practical detection schemes should open applications for these and related one-dimensional structures as NEMS components and ultrasensitive force transducers (98).

Because of their very small size and weight, nanomechanical resonators are theoretically capable of heat detection at the quantum limit and mass sensing at the level of individual molecules. The resonance frequency of a cantilever beam, f_o, scales linearly with the geometric factor t/L^2 (where t is thickness and L the length of the cantilever beam), whereas its mass sensitivity is roughly proportional to f_o^2, so that short light structures provide the highest sensitivity. Husain et al. have demonstrated impressive advances toward fabricating and detecting the motion of ultrahigh-frequency (1 GHz) resonators based on lithographically produced nanowires (99). A recent report of 5.5 fg mass detection using larger Si cantilevers

in ambient conditions (100) heralds the wide use of nanowires in force microscopy, high-frequency circuitry, and calorimetry in the quantum regime.

Nanowire Lasing

Nanowires with flat end facets can be exploited as optical resonance cavities to generate coherent light on the nanoscale. Room temperature UV lasing has been demonstrated in our laboratories for the ZnO and GaN nanowire systems with epitaxial arrays (32), combs (54), and single nanowires (45, 101). ZnO and GaN are wide bandgap semiconductors (3.37, 3.42 eV) suitable for UV-blue optoelectronic applications. The large binding energy for excitons in ZnO (~60 meV) permits lasing via exciton-exciton recombination at low excitation conditions, whereas GaN is known to support an electron-hole plasma (EHP) lasing mechanism. In a series of studies, we have applied far-field imaging and near-field scanning optical microscopy (NSOM) to understand photon confinement in these small ($d \leq \lambda$, where d is the nanowire diameter and λ is the wavelength) cavities.

Well-faceted nanowires with diameters from 100 to 500 nm support predominantly axial Fabry-Perot waveguide modes (separated by $\Delta\lambda = \lambda^2/[2Ln(\lambda)]$, where L is the cavity length and $n(\lambda)$ is the group index of refraction owing to the large diffraction losses suffered by transverse trajectories. Diffraction prevents smaller wires from lasing; PL is lost instead to the surrounding radiation field. ZnO and GaN nanowires produced by VLS growth are cavities with low intrinsic finesse (F) owing to the low reflectivity (R) of their end faces (102) (~19%) [where $F = \pi R^{1/2}/(1\text{-}R)$], such that the confinement time for photons is short and photons travel an average of one to three half-passes before escaping from the cavity. Far-field imaging indicates that PL and lasing emission are localized at the ends of nanowires, which suggests strong waveguiding behavior that is consistent with axial Fabry-Perot modes.

The transition from spontaneous PL to optical gain is achieved by exciting a high density of carriers via pulsed UV illumination. The dependence of nanowire emission on pump power (Figure 11) typically shows three regimes, corresponding to (*a*) spontaneous emission, followed by (*b*) stimulated emission (lasing) above a certain threshold fluence, and (*c*) saturation through gain-pinning at high pump power. The lasing thresholds observed in nanowires vary across several orders of magnitude as a consequence of differing nanowire dimensions, quality of the particular nanowire cavities, and coupling to the substrate (the lowest threshold observed for ZnO is ~70 nJ cm^{-2}; for GaN, ~500 nJ cm^{-2}). The simultaneous appearance of narrow cavity modes (line widths 0.25–1.0 nm) spaced in agreement with cavity dimensions confirms the lasing behavior. The spectral position of the ZnO gain profile is typically nearly independent of pump power at the moderate pumping intensities that correspond to exciton-exciton lasing but exhibits significant red-shift near saturation as band filling and charge screening induce an exciton-to-EHP transition. GaN nanowires, on the other hand, show a consistent red-shift from threshold to saturation owing to band-gap

renormalization. Polarization of the various modes has also been studied (101).

Recent work in our laboratory has focused on two aspects of lasing in one-dimensional ZnO structures: its ultrafast dynamics in nanowires and its manipulation in nanoribbons. Time-resolved second-harmonic generation (TR-SHG) and transient photoluminescence spectroscopy were used (103) to probe carrier relaxation dynamics near the lasing threshold, as well as under gain saturation conditions. Above the lasing threshold, a bi-exponential decay of the PL was observed, with a fast component ($\sim$10 ps) corresponding to exciton-exciton lasing and a slow component ($\sim$70 ps) owing to free exciton spontaneous emission. The fast process shifted to shorter times with increased pumping power, reflecting the increasing influence of EHP dynamics at higher carrier densities (Figure 12). The SHG transient, which monitors the overall repopulation of the valence bands after excitation, showed a fast component with a decay time that decreased from 5 to $\sim$1 ps from threshold to saturation through a multi-body scattering process consisting of both radiative and nonradiative events. In the nanoribbon study (104), we determined the dependence of the lasing threshold and spectrum on the ribbon length by successively etching isolated ribbons using a focused ion beam (FIB). The threshold pump fluence and nanoribbon length were found to be inversely proportional for lengths greater than 10 μm, whereas most ribbons shorter than 5 μm failed to lase at any pump intensity because gain volume was lost.

The most useful applications for nanowire lasers require that they be integrated in circuits and activated by electron-injection rather than optical pumping. Lieber and coworkers have made progress in this direction by assembling *n*-type CdS nanowire Fabry-Perot cavities on *p*-Si wafers to form the required heterojunction for electrically driven lasing (105). More robust assembly methods appropriate to a larger variety of materials will enable the use of injection nanolasers in sensing, optical communications, and probe microscopy.

Phonon Transport

Phonon transport is expected to be greatly impeded in thin (i.e., $d < \Lambda$, where d is the diameter and Λ is the phonon mean free path) one-dimensional nanostructures as a result of increased boundary scattering and reduced phonon group velocities stemming from phonon confinement. Detailed models of phonon heat conduction in cylindrical (106) and rectangular (107) semiconducting nanowires that consider modified dispersion relations and all important scattering processes predict a large decrease (>90%) in the lattice thermal conductivity of wires tens of nanometers in diameter. Size-dependent thermal conductivity in nanostructures presents a major hurdle in the drive toward miniaturization in the semiconductor industry. Yet poor heat transport is advantageous for thermoelectric materials, which are characterized by a figure of merit $\{ZT = a^2T/[\rho(\kappa_p + \kappa_e)]$, with a, T, ρ, κ_p, and κ_e the Seebeck coefficient, absolute temperature, electronic resistivity, lattice thermal conductivity, and electronic thermal conductivity, respectively$\}$ that improves as

phonon transport worsens. A decade ago, the Dresselhaus group predicted that *ZT* can be increased above bulk values in thin nanowires by carefully tailoring their diameters, compositions, and carrier concentrations (108). This remains to be experimentally confirmed.

Several research groups are now fabricating nanowires for thermolelectric (TE) applications. Arrays of Bi_2Te_3 and BiSb wires (109, 110) grown electrochemically in anodic alumina templates and then imbedded in a thermally insulating matrix may soon provide useful TE materials. The enhancement in thermoelectric properties is expected to be most pronounced for zero-dimension quantum-confined structures that feature some means of carrier transport. PbTeSe-based quantum dot array superlattices (111) recently achieved $ZT \sim 2$ at 300 K, compared with $ZT \sim 1$ for the best bulk materials. Well-engineered superlattice nanowires (which integrate a repeating series of nanodots of two different materials along a crystalline wire) may provide even better performance via a combination of sharp periodic band offsets that offer some amount of quantum confinement, high phonon scattering from the nanodot interfaces, and high electrical conductivity (112). Recent work in our laboratories has focused on understanding the thermal transport properties of Si/SiGe superlattice nanowires as the first step in the experimental verification of enhanced *ZT* values in these complex structures (58).

Measurements of the overall thermal conductivity of Si/SiGe superlattice nanowires (113) (Figure 13) were made as a function of temperature (20 to 300 K) and nanowire diameter using a suspended microdevice in vacuum. Individual Si/SiGe wires with a superlattice period of 100–150 nm exhibited a thermal conductivity substantially lower than that of Si/SiGe superlattice films with 30 nm periodicity (10–60% lower, depending on temperature). The broadness of the imbedded Si/SiGe interfaces and the moderate Ge concentration in these wires suggest that alloy (impurity) scattering is the dominant phonon scattering mechanism for short-wavelength phonons, whereas boundary scattering plays a major role in disrupting phonons of all wavelengths. Comparison of superlattice wires with undoped Si nanowires (114) of similar diameter (Figure 13) shows that the former have a conductivity roughly five times smaller at 300 K, or ~500 times less than the bulk conductivity for silicon. Future Seebeck and electronic studies of improved superlattice nanowires are needed to guide the engineering of these materials for TE applications.

Phonon transport in mesoscopic one-dimensional systems was taken near its ultimate limit with the measurement by Roukes and colleagues (115) of the universal quantum of thermal conductance, $G_{th} = \pi^2 k_B^2 T/3h$. They have since gone on to compare the details of phonon scattering in lithographically prepared nanobeams of electrically conducting and insulating materials (116).

Photoconductivity and Chemical Sensing

Electronic conductivity in semiconductor nanowires, belts, and tubes is substantially enhanced by exposing these structures to photons of energy greater than

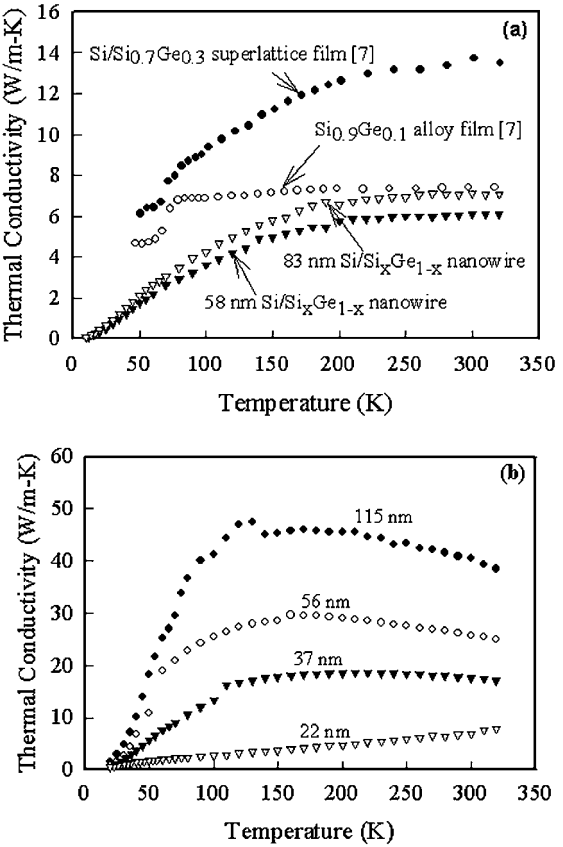

Figure 13 (*a*) Thermal conductivities of 58 nm and 83 nm diameter single crystalline Si/Si_xGe_{1-x} superlattice nanowires. The value of x is ~0.9–0.95 and the superlattice period is from 100–150 nm. Thermal conductivities of a 30 nm period two-dimensional $Si/Si_{0.7}Ge_{0.3}$ superlattice film and $Si_{0.9}Ge_{0.1}$ alloy film (3.5 μm thick) are also shown. (*b*) Thermal conductivities of different diameter single crystalline pure Si nanowires. The number beside each curve denotes the corresponding wire diameter. (Reprinted with permission from Reference 114, copyright AIP, 2003.)

their bandgaps. We demonstrated (117) that photoconductivity in ZnO nanowires could be exploited to create fast and reversible UV optical switches with ON-OFF switching ratios of four to six orders of magnitude under low-intensity 365 nm light. Because the magnitude and decay time of the photoresponse is highly dependent on the presence of ambient O_2, we suggested that the photocurrent in *n*-type oxide nanowires is a product of electron-hole pair formation and electron doping caused by the photo-induced desorption of oxidizing surface species, including oxygen. We went on to utilize the sensitive dependence of nanowire conductivity

on adsorbate molecules to fabricate the first single-crystalline nanowire gas sensor (118). In this work, a SnO_2 nanoribbon bathed in UV light was used to reversibly detect 3–100 ppm NO_2 at room temperature. NO_2 adsorption on the ribbon surface traps free electrons and widens the region of depleted electron density near the surface, thereby causing the conductivity to drop, whereas the UV light continuously desorbs NO_2 to make the sensing dynamic. A series of studies by other groups later extended nanowire-based gas sensing to ZnO belts (119), In_2O_3 wires (120), polycrystalline SnO_2 wires (121), and TiO_2 tubes arrays (122).

Nanowire chemical sensors most often operate via chemical gating induced by the surface adsorption of analyte molecules, although other sensing mechanisms exist (123, 124). The very high surface-to-volume ratios of thin one-dimensional nanostructures endow them with inherently high sensitivity and short response time; however, selectivity is a major problem, especially in the detection of gases. For example, the reactive surfaces of oxide nanowires and carbon nanotubes (CNT) (125) interact with most oxidizing and reducing vapors, which complicates many practical applications. Recently we carried out density functional theory (DFT) calculations to understand the details of molecular adsorption on SnO_2 nanoribbon surfaces (126). We found that (*a*) oxygen chemisorbs only on surfaces that contain oxygen vacancies; (*b*) adsorbed NO_2 exists primarily as tightly bound NO_3 species, a finding that was confirmed with X-ray absorption near-edge spectroscopy (XANES); and (*c*) many surface species are mobile at 300 K and some can oxidize the SnO_2 lattice itself, potentially causing sensor signal drift. Selectivity in nanowire sensors is more easily addressed in liquid media, where ligand-receptor binding (e.g., biotin-streptavidin) and other surface functionalization schemes can provide molecular discrimination (127). It is a good bet that nanowire- and CNT-based chemical sensing will be among the first major commercial applications for one-dimensional nanostructures.

Magnetic Effects

The magnetic properties of solids can exhibit size dependence as a consequence of several effects, including the influence of surfaces, the onset of carrier confinement, and the reduction of structure size below that of a single magnetic domain. It is possible to enhance or even induce magnetic behavior by changing the dimensionality of a system. For example, the broken symmetry of a surface can generate giant magnetic anisotropy energy in magnetic adatoms (128). The study of electron transport in suspended chains of atoms (129) suggests that certain nonmagnetic systems, such as Pd and Pt, become magnetic in such a geometry and behave as ferromagnetic polarized conduction channels (with quantized transport at half a conductance quantum, or e^2/h). Scientific interest in zero-dimension magnetic nanodots centers on the effects of weak structural anisotropy in single-domain particles (130) and their use in biological labeling (131) and assembly into arrays for magnetotransport (132) and high-density data storage (133). Magnetic nanorods

(134) and wires are comparatively recent foci of attention. In addition to exhibiting large anisotropy, one-dimensional magnetic nanostructures can act as their own interconnects, making them attractive for use in sensing and as active elements in spintronic devices.

Size reduction in one-dimensional magnetic nanostructures may alter the magnetic reversal processes of a system, an effect with relevance in data storage and sensing. Most studies on magnetic one-dimensional structures utilize electrodeposited ferromagnetic nanowires grown in large area, variable-density arrays in anodic alumina (AAO), or track-etch templates (135). In general, the large-shape anisotropy of these polycrystalline wires induces a magnetic easy axis parallel to the wire axis and results in high coercivity fields that are inversely proportional to wire diameter (136). Small nanowires behave as single-domain dipoles except in systems with complex magnetocrystalline properties such as cobalt. The mode of magnetic reversal in single wires is diameter dependent, typically crossing over from curling to Stoner-Wohlfarth rotation at a diameter near the magnetic coherence length. In an early study, the magnetic switching of thin nickel wires was shown by micro-superconducting quantum interference device (SQUID) magnetometry (137) to proceed via a nucleation and propagation process rather than by coherent rotation (138) or curling. Micromagnetic modeling of amorphous wires (139) indicates that nucleation of the reversal occurs at the ends of the wire and then traverses the structure as a soliton. Magnetostatic coupling between nanowires in dense arrays causes the square hysteresis loop of single nanowires to narrow and shear. Recent dipole-dipole models (140) and field-dependent magnetic force microscopy (MFM) measurements (141) confirm that the interwire interactions must be reduced if nanowires are to be magnetically addressable as independent data storage elements.

Spintronics requires small structures so that spins act coherently and electrons travel ballistically. Initial work on spin-dependent conductivity in one-dimensional systems has focused on the occurrence of giant magnetoresistance (GMR) in electrodeposited multilayered nanowires (the current perpendicular to plane geometry) (142). Systematic studies of Co/Cu (143), NiFe/Cu (144), and $Ni_{80}Fe_{20}$/Cu nanowires (145) with various repeat schemes have enabled the measurement of interface scattering and spin diffusion lengths in these structures. A nanowire Ni/NiO/Co magnetic tunnel junction was also recently demonstrated (146). However, the field of true one-dimensional nanostructure spintronic devices is in its infancy; nanowires featuring charge-in-plane (CIP) and more complex magnetotransport geometries are now possible (66) but not yet proven.

AAO-templated ferromagnetic nanowires are proving useful in the emerging field of biomagnetics, in which magnetic nanostructures provide a means to sense biomolecules, sort cells, and perform other biological manipulations. For instance, noting that the large remnant magnetization inherent to nanowires permits their use in low-field environments, the Reich group has demonstrated the chemical functionalization of Au/Ni wires for biosensing (147) and developed an approach to magnetically trap (148) single wires in solution.

Electronic Transport

The physics of charge transport in mesoscopic one-dimensional systems is a maturing subject. One striking phenomenon in the mesoscopic domain is the quantization of electrical conductance, which occurs when a quasi-one-dimensional electron gas is made to bridge two electron reservoirs, as in a semiconductor point contact (149), mechanical break junction (150), or carbon nanotube (151). Under ideal ballistic conditions, each spin-degenerate quantum channel contributes a unit of $2e^2/h$ to the electrical conductance. At the time of this writing, all but one of the purported examples of quantized conductance in nanowires were based on chains of metal atoms rather than freestanding, chemically synthesized one-dimensional nanostructures. The observation of quantum transport effects in true metal or semiconductor nanowires requires structures with widths comparable to the Fermi wavelength (typically tens of nm for semiconductors, <1 nm for metals). The difficulty in synthesizing such thin wires and outfitting them with contacts having high transmission coefficients partly explains the dearth of research in this area. However, a recent report (152) of strong Coulomb blockade behavior in monolithic InP nanowires at 0.35 K nicely illustrates the plausibility of the research. This study complements the steps taken toward nanowire-based quantum electronics by Samuelson and coworkers with their demonstration of a resonant tunneling diode (153) and a single electron transistor (154) using individual MBE-grown heterostructure nanowires at temperatures below 12 K. The success of room temperature nanowire quantum devices depends on improved size control, interface engineering, and assembly schemes for these materials.

Nanowire versions of classical electronic devices are well-researched compared with their quantum counterparts. Prototype nanowire field-effect transistors (FETs) include Si (155), InP (156), n-GaN (44), p-GaN (25), In_2O_3 (157), and ZnO (158) examples. In a series of studies over the past few years, the Lieber group pioneered the area of nanowire electronics with the fabrication of locally gated FETs (159), crossed-nanowire *p-n* junctions and LEDs (25), bipolar transistors and inverters (160), and various logic-gate structures and memory elements (161). In general, the performance characteristics of nanowire electronic devices often rival the best bulk and epitaxial single-crystal semiconductors. State-of-the-art nanowire devices employ fluid flow through microscale channels (162, 163) to assemble nanowires into simple crossbar arrays, and electron beam lithography (EBL) to provide electrical contact to the individual wire elements. This fabrication strategy is versatile in that appropriately doped nanowires of a wide variety of optoelectronic materials can be deposited in grid patterns of various geometries to serve desired functions. The use of flexible substrates is also possible (164, 165). However, fluidic assembly suffers from a lack of precision and geometric versatility, whereas EBL is itself tedious and expensive. Complex nanowire electronics cannot be produced economically with the current mixture of bottom-up and top-down construction. To yield a viable technology, breakthroughs must be made in

the true self-assembly of nanowire mixtures into useful architectures. Controlling the placement and connectivity of groups of nanostructures is probably the most monstrous challenge in one-dimensional nanoscience.

Compositionally modulated (heterostructure) nanowires that feature internal *p-n* junctions have enabled the development of single-nanowire LEDs and other devices. Recent examples include VLS-grown Si and GaN nanowire rectifiers (166) and InP nanowire LEDs, as well as rectifying multilayer metal rods fabricated by electrodeposition (167). Modulated nanowires may offer several advantages over their monolithic counterparts in electronic applications, including smaller device sizes, simplified fabrication requirements, and enhanced control over the nature of the active interface. Finally, we note that various aspects of charge transport in both single-component (168) and modulated (169) nanowires recently received theoretical attention.

Ionic Transport

Ionic transport through nanoscale channels is receiving increasing attention owing to recent experiments that report modulation of ion currents during the passage of single molecules of DNA or protein through the protein ion channel α-hemolysin (170). The possibility of rapid DNA sequencing by monitoring the ionic conductance signatures of passing nucleotide oligomers has prompted the synthesis of artificial nanopores (171) and the study of biomolecular transport through them. Nanotubes provide a unique high-aspect-ratio channel in which to study ion transport and fluid flow. A theoretical treatment of ion behavior in gated silica nanotubes (172) suggests that when the tube diameter is smaller than the Debye length, an applied gate bias can completely expel ions of like charge and produce a unipolar solution of counter-ions within the channel. Modifying the surface charge on the nanotube with the gate electrode modulates the ionic current through the tube—the basis for a unipolar ionic field-effect transistor. Also, the 5–20 μm length of the nanotube channels now being fabricated in this laboratory (67) opens up the possibility of imaging and manipulating single molecules as they pass through a tube.

INTEGRATION OF ONE-DIMENSIONAL NANOSTRUCTURES

The key to the future success of one-dimensional nanotechnologies is assembly, or the art of putting nanostructures where one desires, with the desired connectivity, and nowhere else. Nanostructure assembly is challenging because the pertinent length scales prohibit direct tinkering and magnify the disordering effects of electrostatic forces and Brownian motion (173). As we have seen, fluidic assembly schemes offer sufficient control to fabricate simple networks and dictate the macroscopic patterning of nanowires but not with the precision, pattern density, or

complexity needed for many applications. The alignment of nanowires via electric (174) or magnetic (175) forces suffers the additional frustration of fringing fields that make the construction of dense or complex architectures impractical. Lithographic approaches to assembly sidestep some of the above complications but face fundamental challenges in terms of material and geometric versatility. For example, the Heath group recently created nanowire lattices of ultrahigh density and controllable dimensions by transferring prefabricated nanowires from templates to other surfaces (176). Yet it is difficult to extend this or any other physical lithographic scheme beyond the fabrication of grids of identical metal or silicon nanowires. The research community must develop generalized assembly techniques that go well beyond current capabilities if nanowires, rods, belts, and tubes are to see widespread technological application in optoelectronics and computing. All application areas, including those with little or no direct need for assembly, will benefit from advances made in the spatial manipulation of nanostructures.

An attractive nanoscale assembly strategy is cheap, fast, defect tolerant, compatible with a variety of materials in three dimensions, and parallel in nature, ideally utilizing the self-assembly of a mix of one-dimensional elements to generate the core of a device, such as a memory chip or optical display. Self-assembly occurs when the balance of molecular forces within a dynamic system favors the generation of larger-scale spatial linkages and patterns, as in protein folding, the arrangement of surface-functionalized microscopic objects at liquid interfaces (177), and block copolymers that phase-separate to form ordered columnar arrays as thin films (178, 179). However, self-assembly on planar substrates is best suited to the synthesis of isotropic structures with periodic order. This makes exclusive bottom-up (chemical) assembly an unlikely prospect for nanowire layouts that are either spatially asymmetric or require well-defined contacts in order to interface with the macroscopic world.

Perhaps the most realistic approach to practical nanodevices (particularly those not based on regular arrays) is directed assembly, in which some form of lithography—such as EBL, nanoimprint lithography (180), or μ-contact printing (181)—is used to pattern the forces that guide the subsequent bottom-up assembly of nanoscopic units. Progress in the field of directed assembly, although impressive in proving several design concepts, amounts to a series of baby steps on the path to solving a truly daunting problem. Here we highlight recent efforts to assemble one-dimensional nanostructures into useful architectures and practical devices.

It is possible in principle to merge synthesis and assembly into a single step such that systems self-organize as their components grow. Dai and coworkers discovered the potential of self-organization to create electrically connected networks of single-walled carbon nanotubes in a CVD process (182). In this case, nanotubes growing from patterned metal islands wave in the gas stream until encountering and sticking to an adjacent island in a nanoscale game of connect the dots. Nanotubes could also be directed to bridge certain electrodes by applying electric fields in situ during growth. The VLS growth method seems ideally suited to this type of assembly based on lithographically defined growth locations. Yet a

nanowire equivalent to this CNT process has not been reported, perhaps because of the greater stiffness of nanowires compared with CNTs. For now, synthesis and assembly remain separate steps in nanowire device fabrication.

A particularly promising nanofabrication strategy is the use of surface chemistry to direct the assembly of one-dimensional nanostructures onto lithographically patterned substrates. By modifying the surfaces of the nanowires and the substrate with self-assembled monolayers (SAMs), it is possible to control the attractive and repulsive interactions that dictate where and how nanowires attach to the substrate and to each other. These interactions can be of a van der Waals, hydrophobic/hydrophilic, electrostatic, or covalent nature. Mallouk and colleagues have demonstrated the selective adhesion of thick gold nanowires to appropriately functionalized gold surfaces using both electrostatic and covalent linkages in solution (183). In this work, the authors controlled the micron-scale location of groups of nanowires, but not their density or orientation. A subsequent paper from the same laboratory introduced the concept of using the distinct surface chemistry presented by segmented metal nanowires to create two-dimensional or three-dimensional wire superstructures (184). It should be possible to improve the resolution of these techniques to direct individual nanowires to dock in specific locations, perhaps by utilizing ligand-receptor binding or complementary DNA anchoring (185). Ultimately, the practical production of useful architectures will require that mixtures of different types of nanowires having controlled doping profiles and distinct surface binding groups be coaxed to assemble on patterned substrates with high accuracy. Most of the challenges in this area remain to be addressed (186).

Heterostructure nanowires will undoubtedly serve as the preferred building block in directed assembly schemes compared with their monolithic counterparts. In addition to their greater surface functionality, heterostructures incorporate well-controlled interfaces of a quality that is impossible to achieve with multiply crossed nanowires. The various classes of heterostructure nanowires now emerging from several laboratories will simplify assembly requirements, shrink device sizes, and improve device performance.

Another interesting method for arranging vast numbers of one-dimensional nanostructures on solid surfaces is Langmuir-Blodgett (LB) assembly (187). In the LB technique, uniaxial compression of a nanowire-surfactant monolayer floating on an aqueous subphase causes the nanowires to align and pack over a large area (>20 cm^2). The aligned monolayer can then be transferred to a solid surface en masse and with fidelity. Repeated transfers of different types of nanowires can produce functional nanowire lattices (188), although the imprecise registry between layers and the difficulties in providing electrical contacts to individual wires are issues that remain to be addressed. The lattices can be patterned using conventional photolithography to yield arrays of lattice pixels of controlled geometry and pitch. Despite its obvious lack of geometric versatility, LB assembly is the best method available for aligning one-dimensional nanostructures over large areas and with high packing density.

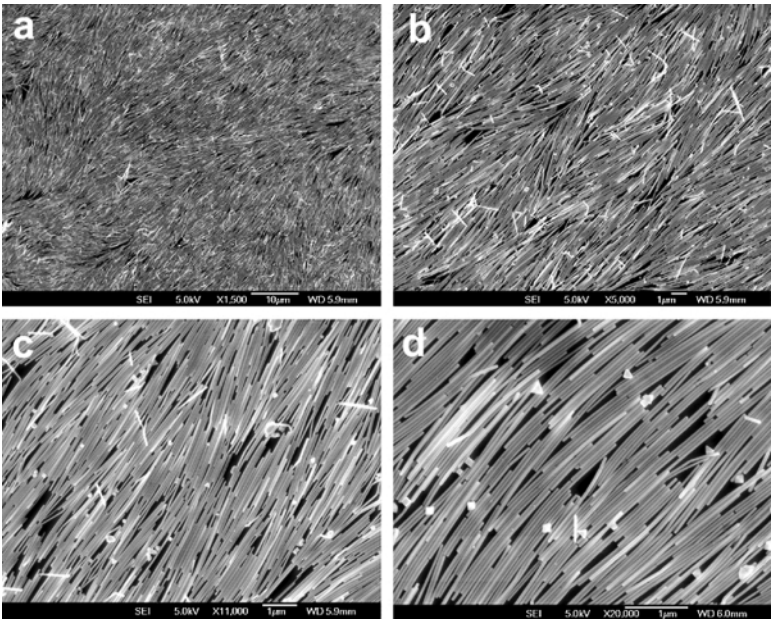

Figure 14 Scanning electron microscopy images of the LB silver nanowire monolayer deposited on a silicon wafer at different magnifications. (Reprinted with permission from Reference 191, copyright Am. Chem. Soc., 2003.)

Examples of functioning devices based on assemblies of one-dimensional nanostructures are only now beginning to appear in the literature. We already discussed the construction of simple LEDs and logic elements from small grids of nanowires. A similar fabrication approach was recently used to create flexible nanowire FETs with a multitude of parallel conduction channels (164). Beyond these electronic examples, a handful of devices reliant on ordered nanowire arrays have been proposed, including nanowire photonic crystals (1), field emission displays (189), and solar cells (190).

We recently used LB assembly to create a molecule-specific chemical sensor based on a monolayer of aligned silver nanowires covering a substrate (Figure 14) (191). The silver wires have well-faceted pentagonal cross sections and sharp pyramidal tips, such that the close-packed nanowire film acts as an excellent substrate for surface-enhanced Raman spectroscopy (SERS) (192) with large electromagnetic field enhancement factors (2×10^5 for thiol and 2,4-dintrotoluene, and 2×10^9 for rhodamine 6G). Both the shape and packing density of the nanowires are vital to the function of this SERS-based sensor. The nanowire monolayer achieves slightly better sensitivities than other types of SERS substrates even without attempts to optimize its performance. This work provides a nice summary of the state-of-the-art in nanostructure assembly: Our current rudimentary capabilities are sometimes sufficient to secure the distinct advantages of one-dimensional

nanostructures, but future assembly techniques will enable greatly superior performance in a range of technologies.

One quite promising application area is nanowire photovoltaics. Organic photovoltaic (PV) devices based on blends of conjugated polymers and inorganic nanostructures are currently objects of intense research for low-cost solar energy conversion. State-of-the-art organic cells (193–195) utilize a bulk heterojunction of donor and acceptor materials to provide a large internal surface area for the efficient charge separation of photo-generated excitons. However, such devices are limited by inefficient charge transport because of the highly folded, discontinuous topology of the donor-acceptor (DA) interface. Replacing the disordered inorganic phase with an aligned array of nanowires can improve charge collection and raise power conversion efficiencies as long as exciton splitting remains efficient. A recent theoretical analysis (196) concluded that nanowire array cells should outperform disordered bulk junction cells when the wire size and interwire spacing become comparable to the exciton diffusion length of the polymer (typically 5–20 nm). Current work focuses on the experimental realization of dense arrays of thin ZnO nanowires for use in nanowire PV cells. In one approach, the ZnO wires are grown in mild aqueous solution on conducting glass substrates and coated with a light-absorbing polythiophene film; deposition of a top electrode then completes the device. Arrays of oxide or chalcogenide nanowires grown with low-cost methods based on seed or template self-assembly are exciting materials for advanced photovoltaics.

CHALLENGES AHEAD

The rapid pace of research in the field of one-dimensional nanostructures is driven by the exciting scientific challenges and technological potential of mesoscopic systems. No fewer than 100 research teams are now active in this young area worldwide. Synthetic capabilities continue to expand quickly, while progress with the difficult tasks of precision property control and assembly inches forward. There are several outstanding scientific challenges in the field that need to be addressed urgently, the most significant of which is the integration and interfacing problem. The ability to create high-density arrays is not enough: How to address individual elements in a high-density array and how to achieve precise layer-to-layer registration for vertical integration are just two of the many challenges still ahead. The achievement of reproducible nanostructural interfaces, semiconductor-semiconductor and metal-semiconductor alike, requires careful examination and understanding of the chemistry and physics occurring at the interface. Equally important is the precise control of the size uniformity, dimensionality, growth direction, and dopant distribution within semiconductor nanostructures, as these structural parameters will ultimately dictate the functionality of the nanostructures. In particular, the physical significance of the dopant distribution and the interfacial junction, and their implications in device operation and performance, will likely require careful re-examination and/or redefinition at the nanometer-length scale. Lastly, accurate

theoretical simulations appropriate to the above-mentioned mesoscopic regime are becoming feasible with the enhanced computing power available and should assist our understanding of many of these size- and dimensionality-controlled phenomena.

We note that the attendant hype from both proponents and opponents of nanotechnology has received increasing attention in the scientific journals (197). Researchers would be responsible and wise to recognize (and work to mitigate) the potential environmental and health hazards of nanoparticles and nanowires. The true danger of these materials stems from their small sizes, reactive surfaces, and high mobility in the environment and perhaps in the body. Some types of nanoparticles are proving to be toxic, and nanowires are obviously reminiscent of asbestos and chrysolite. A systematic evaluation of the environmental and health implications of the large-scale production of these materials is urgently needed. Several reports of limited scope have already been issued (198). We suspect that the environmental and health hazards of one-dimensional nanostructures will prove no more serious or difficult to manage than those of existing particulate sources such as diesel exhaust or asbestos. However, ignoring or dismissing outright the concerns of the public in this or any other area of emerging technology is socially irresponsible unbalanced science.

The *Annual Review of Materials Research* is online at http://matsci.annualreviews.org

LITERATURE CITED

1. Xia YN, Yang PD, Sun YG, Wu YY, Mayers B, et al. 2003. One-dimensional nanostructures: synthesis, characterization, and applications. *Adv. Mater.* 15:353–89
2. Cerrina F, Marrian C. 1996. A path to nanolithography. *MRS Bull.* 21:56–62
3. A special issue on carbon nanotubes. 2002. *Acc. Chem. Res.* 36:997–1113
4. Tenne R. 2003. Advances in the synthesis of inorganic nanotubes and fullerene-like nanoparticles. *Angew. Chem. Int. Ed.* 42:5124–32
5. Weisbuch C, Vinter B, eds. 1991. *Quantum Semiconductor Structures*. Boston: Academic
6. Ohring M, ed. 1992. *The Materials Science of Thin Films*. Boston: Academic
7. Wagner RS, Ellis WC. 1964. Vapor-liquid-solid mechanism of single crystal growth. *Appl. Phys. Lett.* 4:89–90
8. Givargizov EI. 1975. Fundamental aspects of VLS growth. *J. Cryst. Growth* 31:20–30
9. Wu Y, Yang P. 2000. Germanium nanowire growth via simple vapor transport. *Chem. Mater.* 12:605–7
10. Zhang YJ, Zhang Q, Wang NL, Yan YJ, Zhou HH, Zhu J. 2001. Synthesis of thin Si whiskers (nanowires) using $SiCl_4$. *J. Cryst. Growth* 226:185–91
11. Westwater J, Gosain DP, Tomiya S, Usui S, Ruda H. 1997. Growth of silicon nanowires via gold/silane vapor-liquid-solid reaction. *J. Vac. Sci. Technol. B* 15: 554–57
12. Wu Y, Yang P. 2001. Direct observation of vapor-liquid-solid nanowire growth. *J. Am. Chem. Soc.* 123:3165–66
13. Gudiksen MS, Lieber CM. 2000. Diameter-selective synthesis of semiconductor nanowires. *J. Am. Chem. Soc.* 122:8801–2

14. Wu Y, Yan H, Huang M, Messer B, Song JH, Yang P. 2002. Inorganic semiconductor nanowires: rational growth, assembly, and novel properties. *Chem. Eur. J.* 8:1260–68
15. Duan X, Lieber CM. 2000. General synthesis of compound semiconductor nanowires. *Adv. Mater.* 12:298–302
16. Chen CC, Yeh CC, Chen CH, Yu MY, Liu HL, et al. 2001. Catalytic growth and characterization of gallium nitride nanowires. *J. Am. Chem. Soc.* 123:2791–98
17. Zhang J, Peng XS, Wang XF, Wang YW, Zhang LD. 2001. Micro-Raman investigation of GaN nanowires prepared by direct reaction Ga with NH_3. *Chem. Phys. Lett.* 345:372–76
18. He M, Zhou P, Mohammad SN, Harris GL, Halpern JB, et al. 2001. Growth of GaN nanowires by direct reaction of Ga with NH_3. *J. Cryst. Growth* 231:357–65
19. Shi WS, Zheng YF, Wang N, Lee CS, Lee ST. 2001. Synthesis and microstructure of gallium phosphide nanowires. *J. Vac. Sci. Technol. B* 19:1115–18
20. Chen CC, Yeh CC. 2000. Large-scale catalytic synthesis of crystalline gallium nitride nanowires. *Adv. Mater.* 12:738–41
21. Shimada T, Hiruma K, Shirai M, Yazawa M, Haraguchi K, et al. 1998. Size, position and direction control on GaAs and InAs nanowhisker growth. *Superlattice Microstr.* 24:453–58
22. Hiruma K, Yazawa M, Katsuyama T, Ogawa K, Haraguchi K, et al. 1995. Growth and optical properties of nanometer-scale GaAs and InAs whiskers. *J. Appl. Phys.* 77:447–62
23. Yazawa M, Koguchi M, Muto A, Hiruma K. 1993. Semiconductor nanowhiskers. *Adv. Mater.* 5:577–80
24. Kuykendall T, Pauzauskie P, Lee S, Zhang Y, Goldberger J, Yang P. 2003. Metallorganic chemical vapor deposition route to GaN nanowires with triangular cross sections. *Nano Lett.* 3:1063–66
25. Zhong Z, Qian F, Wang D, Lieber CM. 2003. Synthesis of *p*-type gallium nitride nanowires for electronic and photonic nanodevices. *Nano Lett.* 3:343–46
26. Wang Y, Zhang L, Liang C, Wang G, Peng X. 2002. Catalytic growth and photoluminescence properties of semiconductor single-crystal ZnS nanowires. *Chem. Phys. Lett.* 357:314–18
27. Wang Y, Meng G, Zhang L, Liang C, Zhang J. 2002. Catalytic growth of large-scale single-crystal CdS nanowires by physical evaporation and their photoluminescence. *Chem. Mater.* 14:1773–77
28. Lopez-Lopez M, Guillen-Cervantes A, Rivera-Alvarez Z, Hernandez-Calderon I. 1998. Hillock formation during the molecular beam epitaxial growth of ZnSe on GaAs substrates. *J. Cryst. Growth* 193:528–34
29. Peng XS, Meng GW, Wang XF, Wang YW, Zhang J, et al. 2002. Synthesis of oxygen-deficient indium-tin-oxide (ITO) nanofibers. *Chem. Mater.* 14:4490–93
30. Yang P, Lieber CM. 1996, Nanorod-superconductor composites: a pathway to materials with high critical current density. *Science* 273:1836–39
31. Wu XC, Song WH, Zhao B, Sun YP, Du JJ. 2001. Preparation and photoluminescence properties of crystalline GeO_2 nanowires. *Chem. Phys. Lett.* 349:210–14
32. Huang MH, Wu Y, Feick H, Tran N, Weber E, Yang P. 2001. Catalytic growth of zinc oxide nanowires by vapor transport. *Adv. Mater.* 13:113–16
33. Liu X, Li C, Han S, Han J, Zhou C. 2003. Synthesis and electronic transport studies of CdO nanoneedles. *Appl. Phys. Lett.* 82 1950–52
34. Nguyen P, Ng HT, Kong J, Cassell AM, Quinn R, et al. 2003. Epitaxial directional growth of indium-doped tin oxide nanowire arrays. *Nano Lett.* 3:925–28
35. Ma R, Bando Y. 2002. Investigation of the growth of boron carbide nanowires. *Chem. Mater.* 14:4403–7
36. Kim HY, Park J, Yang H. 2003. Direct synthesis of aligned carbide nanowires from

the silicon substrates. *Chem. Commun.* 256–57
37. Kim HY, Park J, Yang H. 2003. Synthesis of silicon nitride nanowires directly from the silicon substrates. *Chem. Phys. Lett.* 372:269–74
38. Stach EA, Pauzauskie PJ, Kuykendall T, Goldberger J, He R, Yang P. 2003. Watching GaN nanowires grow. *Nano Lett.* 3:867–69
39. L'Vov BV. 2000. Kinetics and mechanism of thermal decomposition of GaN. *Thermochim. Acta* 360:85–91
40. Munir ZA, Searcy AW. 1965. Activation energy for the sublimation of gallium nitride. *J. Chem. Phys.* 42:4223–28
41. Koleske DD, Wickenden AE, Henry RL, Culbertson JC, Twigg ME. 2001. GaN decomposition in H_2 and N_2 at MOVPE temperatures and pressures. *J. Cryst. Growth* 223:466–83
42. Zhou SM, Feng YS, Zhang LD. 2003. A physical evaporation synthetic route to large-scale GaN nanowires and their dielectric properties. *Chem. Phys. Lett.* 369:610–14
43. Duan X, Lieber CM. 2000. Laser-assisted catalytic growth of single crystal GaN nanowires. *J. Am. Chem. Soc.* 122:188–89
44. Huang Y, Duan X, Cui Y, Lieber CM. 2002. Gallium nitride nanowire nanodevices. *Nano Lett.* 2:101–4
45. Johnson JC, Choi H-J, Knutsen KP, Schaller RD, Yang P, Saykally RJ. 2002. Single gallium nitride nanowire lasers. *Nat. Mater.* 1:106–10
46. Choi H-J, Johnson JC, He R, Lee S-K, Kim F, et al. 2003. Self-organized GaN quantum wire UV lasers. *J. Phys. Chem. B* 107:8721–25
47. Seo HW, Bae SY, Park J, Yang H, Park KS, Kim S. 2002. Strained gallium nitride nanowires. *J. Chem. Phys.* 116:9492–99
48. Kim H-M, Kang TW, Chung KS. 2003. Nanoscale ultraviolet-light-emitting diodes using wide-bandgap gallium nitride nanorods. *Adv. Mater.* 15:567–69
49. Dai ZR, Pan ZW, Wang ZL. 2003. Novel nanostructures of functional oxides synthesized by thermal evaporation. *Adv. Func. Mater.* 13:9–24
50. Frank FC. 1949. The influence of dislocations on crystal growth. *Discuss. Faraday Soc.* 23:48–54
51. Zhang R-Q, Lifshitz Y, Lee S-T. 2003. Oxide-assisted growth of semiconducting nanowires. *Adv. Mater.* 15:635–40
52. Pan ZW, Dai ZR, Wang ZL. 2001. Nanobelts of semiconducting oxides. *Science* 291:1947–49
53. Yan H, He R, Pham J, Yang P. 2003. Morphogenesis of one-dimensional ZnO nano- and microcrystals. *Adv. Mater.* 15:402–5
54. Yan H, He R, Johnson J, Law M, Saykally RJ, Yang P. 2003. Dendrite nanowire UV laser array. *J. Am. Chem. Soc.* 125:4728–29
55. Sun Y, Yin Y, Mayers BT, Herricks T, Xia Y. 2002. Uniform silver nanowires synthesis by reducing $AgNO_3$ with ethylene glycol in the presence of seeds and poly(vinyl pyrrolidone). *Chem. Mater.* 14:4736–45
56. Vayssieres L, Keis K, Lindquist S-E, Hagfeldt A. 2001. Purpose-built anisotropic metal oxide material: three-dimensional highly oriented microrod array of ZnO. *J. Phys. Chem. B* 105:3350–52
57. Greene LE, Law M, Goldberger J, Kim F, Johnson JC, et al. 2003. Low-temperature wafer-scale production of ZnO nanowire arrays. *Angew. Chem. Int. Ed.* 42:3031–34
58. Wu Y, Fan R, Yang P. 2002. Block-by-block growth of single-crystalline Si/SiGe superlattice nanowires. *Nano Lett.* 2:83–86
59. Gudiksen MS, Lauhon UJ, Wang J, Smith DC, Lieber CM. 2002. Growth of nanowire superlattice structures for nanoscale photonics and electronics. *Nature* 415:617–20
60. Bjoerk MT, Ohlsson BJ, Sass T, Persson AI, Thelander C, et al. 2002.

One-dimensional steeplechase for electrons realized. *Nano Lett.* 2:87–89
61. Solanki R, Huo J, Freeouf JL, Miner B. 2002. Atomic layer deposition of ZnSe/CdSe superlattice nanowires. *Appl. Phys. Lett.* 81:3864–66
62. Keating CD, Natan MJ. 2003. Striped metal nanowires as building blocks and optical tags. *Adv. Mater.* 15:451–54
63. Valizadeh S, Hultman L, George J-M, Leisner P. 2002. Template synthesis of Au/Co multilayered nanowires by electrochemical deposition. *Adv. Func. Mater.* 12:766–72
64. Goldberger J, He R, Zhang Y, Lee S, Yan H, et al. 2003. Single-crystal gallium nitride nanotubes. *Nature* 422:599–602
65. Lauhon LJ, Gudiksen MS, Wang D, Lieber CM. 2002. Epitaxial core-shell and core-multishell nanowire heterostructures. *Nature* 420:57–61
66. He R, Law M, Fan R, Kim F, Yang P. 2002. Functional bimorph composite nanotapes. *Nano Lett.* 2:1109–12
67. Fan R, Wu Y, Li D, Yue M, Majumdar A, Yang P. 2003. Fabrication of silica nanotube arrays from vertical silicon nanowire templates. *J. Am. Chem. Soc.* 125:5254–55
68. Wu Q, Hu Z, Wang X, Lu Y, Chen X, et al. 2003. Synthesis and characterization of faceted hexagonal aluminum nitride nanotubes. *J. Am. Chem. Soc.* 125:10176–77
69. Li Y, Bando Y, Golberg D. 2003. Single-crystalline In_2O_3 nanotubes filled with In. *Adv. Mater.* 15:581–85
70. Yu H, Li J, Loomis RA, Wang L-W, Buhro WE. 2003. Two- versus three-dimensional quantum confinement in indium phosphide wires and dots. *Nat. Mater.* 2:517–20
71. Murray CB, Kagan CR, Bawendi MG. 2000. Synthesis and characterization of monodisperse nanocrystals and close-packed nanocrystal assemblies. *Annu. Rev. Mater. Sci.* 30:545–610
72. Li L-S, Hu J, Yang W, Alivisatos PA. 2001. Band gap variation of size- and shape-controlled colloidal CdSe quantum rods. *Nano Lett.* 1:349–51
73. Kan S, Mokari T, Rothenberg E, Banin U. 2003. Synthesis and size-dependent properties of zinc-blende semiconductor quantum rods. *Nat. Mater.* 2:155–58
74. Gudiksen MS, Wang J, Lieber CM. 2002. Size-dependent photoluminescence from single indium phosphide nanowires. *J. Phys. Chem. B* 106:4036–39
75. Wang J, Gudiksen MS, Duan X, Cui Y, Lieber CM. 2001. Highly polarized photoluminescence and photodetection from single indium phosphide nanowires. *Science* 293:1455–57
76. Qi J, Belcher AM, White JM. 2003. Spectroscopy of individual silicon nanowires. *Appl. Phys. Lett.* 82:2616–18
77. Huynh WU, Dittmer JJ, Alivisatos AP. 2002. Hybrid nanorod-polymer solar cells. *Science* 295:2425–27
78. Manna L, Milliron DJ, Meisel A, Scher EC, Alivisatos AP. 2003. Controlled growth of tetrapod-branched inorganic nanocrystals. *Nat. Mater.* 2:382–85
79. Park, WI, Yi G-C, Kim M, Pennycook SJ. 2003. Quantum confinement observed in ZnO/ZnMgO nanorod heterostructures. *Adv. Mater.* 15:526–29
80. Schiøtz J, Jacobsen KW. 2003. A maximum in the strength of nanocrystalline copper. *Science* 301:1357–59
81. Hasmy A, Medina E. 2002. Thickness induced structural transition in suspended fcc metal nanofilms. *Phys. Rev. Lett.* 88:096103
82. Diao J, Gall K, Dunn ML. 2003. Surface-stress-induced phase transformation in metal nanowires. *Nat. Mater.* 2:656–60
83. Buffat P, Borel J-P. 1976. Size effect on the melting temperature of gold particles. *Phys. Rev. A* 13:2287–98
84. Gülseren O, Ercolessi F, Tosatti E. 1995. Premelting of thin wires. *Phys. Rev. B* 51:7377–80
85. Schmidt M, Kusche R, von Issendorff B, Haberland H. 1998. Irregular variations in

the melting point of size-selected atomic clusters. *Nature* 393:238–40
86. Link S, Burda C, Mohamed MB, Nikoobakht B, El-Sayed MA. 1999. Laser photothermal melting and fragmentation of gold nanorods: energy and laser pulse-width dependence. *J. Phys. Chem. A* 103:1165–70
87. Link S, Wang ZL, El-Sayed MA. 2000. How does a gold nanorod melt? *J. Phys. Chem. B* 104:7867–70
88. Wu Y, Yang P. 2001. Melting and welding semiconductor nanowires in nanotubes. *Adv. Mater.* 13:520–23
89. Christenson HK. 2001. Confinement effects on freezing and melting. *J. Phys. Condens. Matter* 13:R95–133
90. Deleted in proof
91. Wong WW, Sheehan PE, Lieber CM. 1997. Nanobeam mechanics: elasticity, strength, and toughness of nanorods and nanotubes. *Science* 277:1971–75
92. Kis A, Mihailovic D, Remskar M, Mrzel A, Jesih A, et al. 2003. Shear and Young's moduli of MoS_2 nanotube ropes. *Adv. Mater.* 15:733–36
93. Wang ZL, Dai ZR, Gao RP, Bai ZG, Gole JL. 2000. Side-by-side silicon carbide-silica biaxial nanowires: synthesis, structure, and mechanical properties. *Appl. Phys. Lett.* 77:3349–51
94. Bai XD, Gao PX, Wang ZL, Wang EG. 2003. Dual-mode mechanical resonance of individual ZnO nanobelts. *Appl. Phys. Lett.* 82:4806–8
95. Zhang H-F, Wang C-M, Buck EC, Wang L-S. 2003. Synthesis, characterization, and manipulation of helical SiO_2 nanosprings. *Nano Lett.* 3:577–80
96. Gu G, Schmid M, Chiu P-W, Minett A, Fraysse J, et al. 2003. V_2O_5 nanofibre sheet actuators. *Nat. Mater.* 2:316–19
97. Deleted in proof
98. Kawakatsu H, Kawai S, Saya D, Nagashio M, Kobayashi D, et al. 2002. Towards atomic force microscopy up to 100 MHz. *Rev. Sci. Instrum.* 73:2317–20
99. Husain A, Hone J, Postma HWC, Huang XMH, Drake T, et al. 2003. Nanowire-based very-high-frequency electromechanical resonator. *Appl. Phys. Lett.* 83:1240–42
100. Lavrik NV, Datskos PG. 2003. Femtogram mass detection using photothermally actuated nanomechanical resonators. *Appl. Phys. Lett.* 82:2697–99
101. Johnson JC, Yan H, Yang P, Saykally RJ. 2003. Optical cavity effects in ZnO nanowire lasers and waveguides. *J. Phys. Chem. B* 107:8816–28
102. Maslov AV, Ning CZ. 2003. Reflection of guided modes in a semiconductor nanowire laser. *Appl. Phys. Lett.* 83:1237–39
103. Johnson JC, Knutsen KP, Yan H, Law M, Yang P, Saykally RJ. 2003. Ultrafast carrier dynamics in single ZnO nanowire and nanoribbon lasers. *Nano Lett.* Published online on 11/26/03
104. Yan H, Johnson J, Law M, He R, Knutsen KP, et al. 2003. ZnO nanoribbon microcavity lasers. *Adv. Mater.* 15:1907–11
105. Duan X, Huang Y, Agarwai R, Lieber CM. 2003. Single-nanowire electrically driven lasers. *Nature* 421:241–45
106. Zou J, Balandin A. 2001. Phonon heat conduction in a semiconductor nanowire. *J. Appl. Phys.* 89:2932–38
107. Lü X, Chu JH, Shen WZ. 2003. Modification of the lattice thermal conductivity in semiconductor rectangular nanowires. *J. Appl. Phys.* 93:1219–29
108. Hicks LD, Dresselhaus MS. 1993. Effect of quantum well structures on the thermoelectric figure of merit. *Phys. Rev. B* 47:12727–31
109. Martín-González M, Snyder GJ, Prieto AL, Gronsky R, Sands T, Stacy AM. 2003. Direct electrodeposition of highly dense 50 nm $Bi_2Se_{3-y}Te_y$ nanowire arrays. *Nano Lett.* 3:973–77
110. Prieto AL, Martín-González M, Kenayi J, Gronsky R, Sands T, Stacy AM. 2003. The electrodeposition of high-density, ordered arrays of $Bi_{1-x}Sb_x$ nanowires. *J. Am. Chem. Soc.* 125:2388–89

111. Harman TC, Taylor PJ, Walsh MP, LaForge BE. 2002. Quantum dot superlattice thermoelectric materials and devices. *Science* 297:2229–32
112. Lin Y-M, Dresselhaus MS. 2003. Thermoelectric properties of superlattice nanowires. *Phys. Rev. B* 68:075304
113. Li D, Wu Y, Fan R, Yang P, Majumdar A. 2003. Thermal conductivity of Si/SiGe superlattice nanowires. *Appl. Phys. Lett.* 83:3186–88
114. Li D, Wu Y, Kim P, Shi L, Yang P, Majumdar A. 2003. Thermal conductivity of individual silicon nanowires. *Appl. Phys. Lett.* 83:2934–36
115. Schwab K, Henriksen EA, Worlock JM, Roukes ML. 2000. Measurement of the quantum of thermal conductance. *Nature* 404:974–77
116. Fon W, Schwab KC, Worlock JM, Roukes ML. 2002. Phonon scattering mechanisms in suspended nanostructures from 4 to 40 K. *Phys. Rev. B* 66:045302
117. Kind H, Yan H, Law M, Messer B, Yang P. 2002. Nanowire UV photodetectors and optical switches. *Adv. Mater.* 14:158–60
118. Law M, Kind H, Kim F, Messer B, Yang P. 2002. NO_2 photochemical sensing with SnO_2 nanoribbons at room temperature. *Angew. Chem. Int. Ed.* 41:2405–8
119. Comini E, Faglia G, Sberveglieri G, Pan Z, Wang ZL. 2002. Stable and highly sensitive gas sensors based on semiconducting oxide nanobelts. *Appl. Phys. Lett.* 81:1869–71
120. Li C, Zhang D, Liu X, Han S, Tang T, Han J, Zhou C. 2003. In_2O_3 nanowires as chemical sensors. *Appl. Phys. Lett.* 82:1613–15
121. Kolmakov A, Zhang Y, Cheng G, Moskovits M. 2003. Detection of CO and O_2 using tin oxide nanowire sensors. *Adv. Mater.* 15:997–1000
122. Varghese OK, Gong D, Paulose M, Ong KG, Dickey EC, Grimes CA. 2003. Extreme changes in the electrical resistance of titania nanotubes with hydrogen exposure. *Adv. Mater.* 15:624–27
123. Favier F, Walter EC, Zach MP, Benter T, Penner RM. 2001. Hydrogen sensors and switches from electrodeposited palladium mesowire arrays. *Science* 293:2227–31
124. Li CZ, He X, Bogozi A, Bunch JS, Tao NJ. 2000. Molecular detection based on conductance quantization of nanowires. *Appl. Phys. Lett.* 76:1333–35
125. Kong J, Dai HJ. 2001. Full and modulated gating of individual carbon nanotubes by organic amine compounds. *J. Phys. Chem. B* 105:2890–93
126. Maiti A, Rodriguez JA, Law M, Kung P, McKinney JR, Yang P. 2003. SnO_2 nanoribbons as NO_2 sensors: insights from first principles calculations. *Nano Lett.* 3:1025–28
127. Cui Y, Wei Q, Park H, Lieber CM. 2001. Nanowire nanosensors for highly sensitive and selective detection of biological and chemical species. *Science* 293:1289–92
128. Gambardella P, Rusponi S, Veronese M, Dhesi SS, Grazioli C, et al. 2003. Giant magnetic anisotropy of single cobalt atoms and nanoparticles. *Science* 300:1130–33
129. Rodrigues V, Bettini J, Silva PC, Ugarte D. 2003. Evidence for spontaneous spin-polarized transport in magnetic nanowires. *Phys. Rev. Lett.* 91:096801
130. Puntes VF, Krishnan KM, Alivisatos AP. 2001. Colloidal nanocrystal shape and size control: the case of cobalt. *Science* 291:2115–17
131. Lewin M, Carlesso N, Tung C-H, Tang X-W, Cory D, et al. 2000. Tat peptide-derivatized magnetic nanoparticles allow in vivo tracking and recovery of progenitor cells. *Nat. Biotechnol.* 18:410–14
132. Black CT, Murray CB, Sandstrom RL, Sun S. 2000. Spin-dependent tunneling in self-assembled cobalt-nanocrystal superlattices. *Science* 290:1131–34
133. Anders S, Toney MF, Thomson T, Thiele J-U, Terris BD, et al. 2003. X-ray studies of magnetic nanoparticle assemblies. *J. Appl. Phys.* 93:7343–45

134. Cordente N, Respaud M, Senocq F, Casanove M-J, Amiens C, Chaudret B. 2001. Synthesis and magnetic properties of nickel nanorods. *Nano Lett.* 1:565–68
135. Sellmyer DJ, Zheng M, Skomski R. 2001. Magnetism of Fe, Co and Ni nanowires in self-assembled arrays. *J. Phys. Condens. Matter* 13:R433–60
136. Han GC, Zong BY, Luo P, Wu YH. 2003. Angular dependence of the coercivity and remanence of ferromagnetic nanowire arrays. *J. Appl. Phys.* 93:9202–7
137. Wernsdorfer W, Doudin B, Mailly D, Hasselbach K, Benoit A, et al. 1996. Nucleation of magnetization reversal in individual nanosized nickel wires. *Phys. Rev. Lett.* 77:1873–76
138. Martin JI, Nogués J, Schuller IK, Van Bael MJ, Temst K, et al. 1998. Magnetization reversal in long chains of submicrometric Co dots. *Appl. Phys. Lett.* 72:255–57
139. Hertel R. 2001. Micromagnetic simulations of magnetostatically coupled nickel nanowires. *J. Appl. Phys.* 90:5752–58
140. Fodor PS, Tsoi GM, Wenger LE. 2003. Modeling of hysteresis and magnetization curves for hexagonally ordered electrodeposited nanowires. *J. Appl. Phys.* 93:7438–40
141. Sorop TG, Untiedt C, Luis F, Kröll M, Rasa M, de Jongh LJ. 2003. Magnetization reversal of ferromagnetic nanowires studied by magnetic force microscopy. *Phys. Rev. B* 67:014402
142. Zhuravlev MY, Lutz HO, Vedyayev AV. 2001. Size effects in the giant magnetoresistive of segmented nanowires. *Phys. Rev. B* 63:174409
143. Piraux L, George JM, Despres JF, Leroy C, Ferain E, et al. 1994. Giant magnetoresistance in magnetic multilayered nanowires. *Appl. Phys. Lett.* 65:2484–86
144. Dubois S, Marchal C, Beuken JM, Piraux L, Duvail JL, et al. 1997. Perpendicular giant magnetoresistance of NiFe/Cu multilayered nanowires. *Appl. Phys. Lett.* 70:396–98
145. Dubois S, Piraux L, George JM, Ounadjela K, Duvail JL, Fert A. 1999. Evidence for a short spin diffusion length in permalloy from the giant magnetoresistance of multilayered nanowires. *Phys. Rev. B* 60:477–84
146. Sokolov A, Sabirianov IF, Tsymbal EY, Doubin B, Li XZ, Redepenning J. 2003. Resonant tunneling in magnetoresistive Ni/NiO/Co nanowire junctions. *J. Appl. Phys.* 93:7029–31
147. Reich DH, Tanase M, Hultgren A, Bauer LA, Chen CS, Meyer GJ. 2003. Biological applications of multifunctional magnetic nanowires. *J. Appl. Phys.* 93:7275–80
148. Tanase M, Silevitch DM, Hultgren A, Bauer LA, Searson PC, et al. 2002. Magnetic trapping and self-assembly of multicomponent nanowires. *J. Appl. Phys.* 91:8549–51
149. van Wees BJ, van Houten H, Beenakker CWJ, Williamson JG, Kouwenhoven LP, et al. 1988. Quantized conductance of point contacts in a two-dimensional electron gas. *Phys. Rev. Lett.* 60:848–50
150. Muller CJ, van Ruitenbeek JM, de Jongh LJ. 1992. Conductance and supercurrent discontinuities in atomic-scale metallic constrictions of variable width. *Phys. Rev. Lett.* 69:140–43
151. Frank S, Poncharal P, Wang ZL, de Heer WA. 1998. Carbon nanotube quantum resistors. *Science* 280:1744–46
152. De Franceschi S, van Dam JA, Bakkers EPAM, Feiner LF, Gurevich L, Kouwenhoven LP. 2003. Single-electron tunneling in InP nanowires. *Appl. Phys. Lett.* 83:344–46
153. Björk MT, Ohlsson BJ, Thelander C, Persson AI, Deppert K, et al. 2002. Nanowire resonant tunneling diodes. *Appl. Phys. Lett.* 81:4458–60
154. Thelander C, Mårtensson T, Björk MT, Ohlsson BJ, Larsson MW, et al. 2003. Single-electron transistors in heterostructure nanowires. *Appl. Phys. Lett.* 83:2052–54

155. Chung S-W, Yu J-Y, Heath JR. 2000. Silicon nanowire devices. *Appl. Phys. Lett.* 76:2068–70
156. Duan X, Huang Y, Cui Y, Wang J, Lieber CM. 2001. Indium phosphide nanowires as building blocks for nanoscale electronic and optoelectronic devices. *Nature* 409:66–69
157. Zhang D, Li C, Han S, Liu X, Tang T, et al. 2003. Electronic transport studies of single-crystalline In_2O_3 nanowires. *Appl. Phys. Lett.* 82:112–14
158. Arnold MS, Avouris P, Pan ZW, Wang ZL. 2003. Field-effect transistors on single semiconducting oxide nanobelts. *J. Phys. Chem. B* 107:659–63
159. Huang Y, Duan X, Cui Y, Lauhon LJ, Kim K-H, Lieber CM. 2001. Logic gates and computation from assembled nanowires building blocks. *Science* 294:1313–17
160. Cui Y, Lieber CM. 2001. Functional nanoscale electronic devices assembled using silicon nanowire building blocks. *Science* 291:851–53
161. Duan X, Huang Y, Lieber CM. 2002. Nonvolatile memory and programmable logic from molecule-gated nanowires. *Nano Lett.* 2:487–90
162. Messer B, Song JH, Yang P. 2000. Microchannel networks for nanowires patterning. *J. Am. Chem. Soc.* 122:10232–33
163. Huang Y, Duan X, Wei Q, Lieber CM. 2001. Directed assembly of one-dimensional nanostructures into functional networks. *Science* 291:630–33
164. Duan X, Niu C, Sahi V, Chen J, Parce JW, et al. 2003. High-performance thin-film transistors using semiconductor nanowires and nanoribbons. *Nature* 425:274–78
165. McAlpine MC, Friedman RS, Jin S, Lin K, Wang WU, Lieber CM. 2003. High-performance nanowire electronics and photonics on glass and plastic substrates. *Nano Lett.* 3:1531–35
166. Cheng G, Kolmakov A, Zhang Y, Moskovits M, Munden R, et al. 2003. Current rectification in a single GaN nanowire with a well-defined *p-n* junction. *Appl. Phys. Lett.* 83:1578–80
167. Kovtyukhova NI, Martin BR, Mbindyo JKN, Smith PA, Razavi B, et al. 2001. Layer-by-layer assembly of rectifying junctions in and on metal nanowires. *J. Phys. Chem. B* 105:8762–69
168. Rotkin SV, Ruda HE, Shik A. 2003. Universal description of channel conductivity for nanotube and nanowire transistors. *Appl. Phys. Lett.* 83:1623–25
169. Yan Voon LCL, Willatzen M. 2003. Electron states in modulated nanowires. *J. Appl. Phys.* 93:9997–10000
170. Meller A, Nivon L, Brandin E, Golovchenko J, Branton D. 2000. Rapid nanopore discrimination between single polynucleotide molecules. *Proc. Natl. Acad. Sci. USA* 97:1079–84
171. Li J, Stein D, McMullan C, Branton D, Aziz MJ, Golovchenko J. 2001. Ion-beam sculpting at nanometre length scales. *Nature* 412:166–69
172. Daiguji H, Yang P, Majumdar A. 2003. Ion transport in nanofluidic channels. *Nano Lett.* 4:137–142
173. Service R. 2001. Assembling nanocircuits from the bottom up. *Science* 293:782–85
174. Smith PA, Nordquist CD, Jackson TN, Mayer TS, Martin BR, et al. 2000. Electric-field assisted assembly and alignment of metallic nanowires. *Appl. Phys. Lett.* 77:1399–401
175. Tanase M, Bauer LA, Hultgren A, Silevitch DM, Sun L, et al. 2001. Magnetic alignment of fluorescent nanowires. *Nano Lett.* 1:155–58
176. Melosh NA, Boukai A, Diana F, Gerardot B, Badolato A, et al. 2003. Ultrahigh-density nanowire lattices and circuits. *Science* 300:112–15
177. Whitesides GM, Boncheva M. 2002. Beyond molecules: self-assembly of mesoscopic and macroscopic components. *Proc. Natl. Acad. Sci. USA* 99:4769–74
178. Guarini KW, Black CT, Zhang Y, Kim H, Sikorski EM, Babich IV. 2002. Process integration of self-assembled polymer

templates into silicon nanofabrication. *J. Vac. Sci. Technol. B* 20:2788–92
179. Ludwigs S, Böker A, Voronov A, Rehse N, Magerle R, Krausch G. 2003. Self-assembly of functional nanostructures from ABC triblock copolymers. *Nat. Mater.* 2:744–47
180. Chou SY, Krauss PR, Renstrom PJ. 1995. Imprint of sub-25 nm vias and trenches in polymers. *Appl. Phys. Lett.* 67:3114–16
181. Xia Y, Whitesides GM. 1998. Soft lithography. *Annu. Rev. Mater. Sci.* 28:153–84
182. Dai H. 2002. Carbon nanotubes: synthesis, integration, and properties. *Acc. Chem. Res.* 35:1035–44
183. Martin BR, St. Angelo SK, Mallouk TE. 2002. Interactions between suspended nanowires and patterned surfaces. *Adv. Funct. Mater.* 12:759–65
184. Kovtyukhova NI, Mallouk TE. 2002. Nanowires as building blocks for self-assembling logic and memory circuits. *Chem. Eur. J.* 8:4355–63
185. Mirkin CA, Letsinger RL, Mucic RC, Storhoff JJ. 1996. A DNA-based method for rationally assembling nanoparticles into macroscopic materials. *Nature* 382:607–9
186. Marrian CRK, Tennant DM. 2003. Nanofabrication. *J. Vac. Sci. Technol. A* 21:S207–15
187. Yang P. 2003. Wires on water. *Nature* 425:243–44
188. Whang D, Jin S, Wu Y, Lieber CM. 2003. Large-scale hierarchical organization of nanowire arrays for integrated nanosystems. *Nano Lett.* 3:1255–59
189. Kim H-M, Kang TW, Chung KS, Hong JP, Choi WB. 2003. Field emission displays of wide-bandgap gallium nitride nanorod arrays grown by hydride vapor phase epitaxy. *Chem. Phys. Lett.* 377:491–94
190. Wu Y, Yan H, Yang P. 2002. Semiconductor nanowire array: potential substrates for photocatalysis and photovoltaics. *Top. Catal.* 19:197–202
191. Tao A, Kim F, Hess C, Goldberger J, He R, et al. 2003. Langmuir-Blodgett silver nanowire monolayers for molecular sensing using surface-enhanced raman spectroscopy. *Nano Lett.* 3:1229–33
192. Kneipp K, Kneipp H, Itzkan I, Dasari RR, Feld MS. 2002. Surface-enhanced Raman scattering and biophysics. *J. Phys. Condens. Matter* 14:R597–624
193. Shaheen SE, Brabec CJ, Sariciftci NS, Padinger F, Fromherz T, Hummelen JC. 2001. 2.5% efficient organic plastic solar cells. *Appl. Phys. Lett.* 78:841–43
194. Gregg BA. 2003. Excitonic solar cells. *J. Phys. Chem. B* 107:4688–98
195. Peumans P, Yakimov A, Forrest SR. 2003. Small molecular weight organic thin-film photodetectors and solar cells. *J. Appl. Phys.* 93:3693–723
196. Kannan B, Castelino K, Majumdar A. 2003. Design of nanostructured heterojunction polymer photovoltaic devices. *Nano Lett.* 3:1729–32
197. Brumfiel G. 2003. A little knowledge. *Nature* 424:246–48
198. Dagani R. 2003. Nanomaterials: safe or unsafe? *C&EN News* 81:30–33

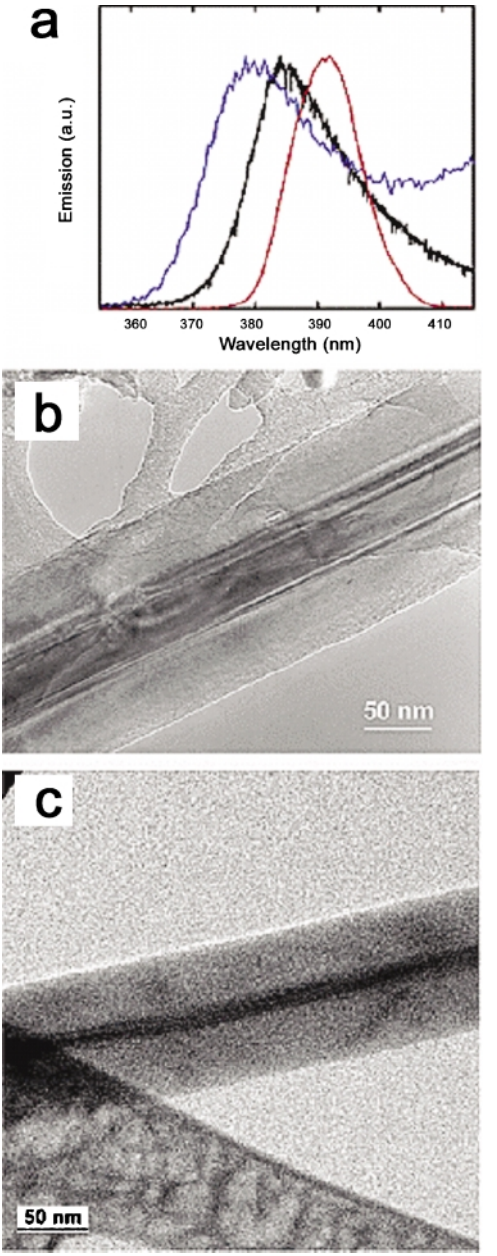

See legend on next page

Figure 9 Core-sheath nanowire light emission. (*a*) Photoluminescence (PL) spectra of $GaN/Al_xGa_{1-x}N$ core-sheath heterostructure nanowires with core sizes of 20 nm (*blue line*) and 52 nm (*black line*), and monolithic GaN nanowire PL (*red line*) for comparison. (*b*) TEM image of the heterostructure nanowire with a core size of 52 nm. (*c*) TEM image of the heterostructure nanowire with a core size of 20 nm. PL measurements were made with an unpolarized He-Cd laser, operating at 325 nm. (Reprinted with permission from Reference 46, copyright Am. Chem.Soc. 2003.)

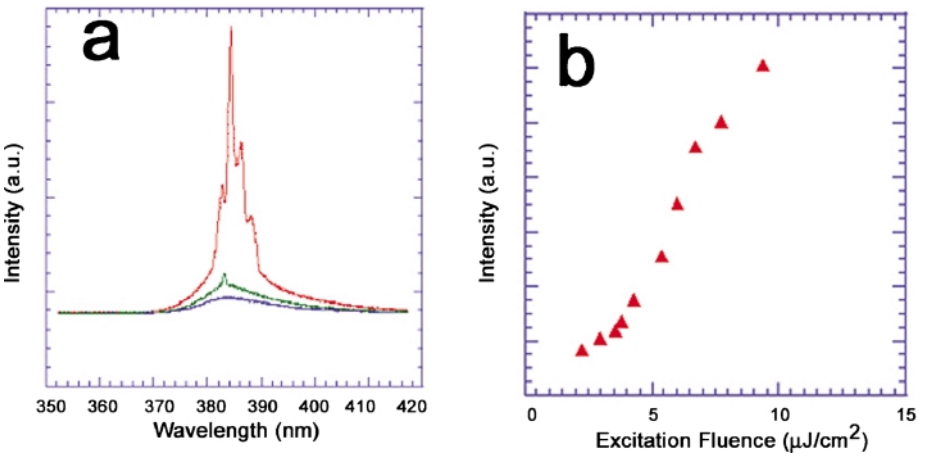

Figure 11 (*a*) Spectra of light emission from GaN/AlGaN core-sheath nanowires below, near and above threshold (about 2–3 $\mu J/cm^2$). (*b*) The power dependence of output integrated emission intensity. (Reprinted with permission from Reference 46, copyright Am. Chem. Soc., 2003.)

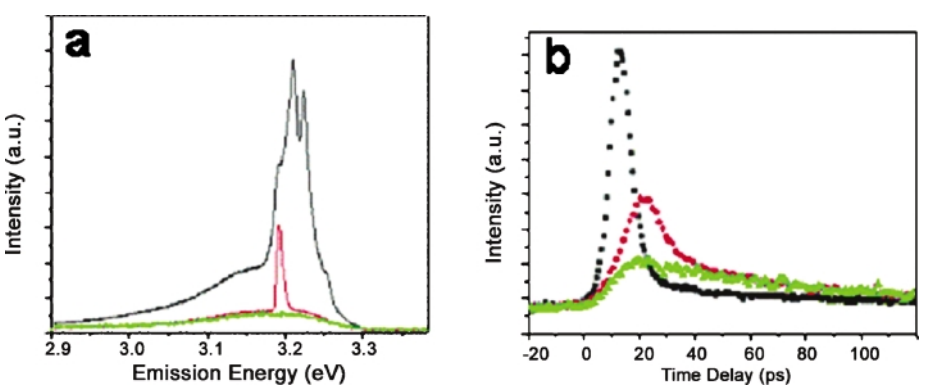

Figure 12 (*a*) PL/lasing spectra of single ZnO nanowire near the lasing threshold (excitation ~1 $\mu J/cm^2$) and (*b*) transient PL response. Long decay component is 70 ± 7 ps and short component is 9 ± 0.8 ps (*red*) and 4.0 ± 0.3 ps (*black*). (Reprinted with permission from Reference 103, copyright Am.Chem. Soc., 2003.)

Annual Review of Materials Research
Volume 34, 2004

CONTENTS